

Pacific Northwest National Laboratory

Operated by Battelle for the
U.S. Department of Energy

Seismic Event-Induced Waste Response and Gas Mobilization Predictions for Typical Hanford Waste Tank Configurations

H. C. Reid
J. E. Deibler

RECEIVED
OCT 10 1997
OSTI

September 1997

Prepared for the U.S. Department of Energy
under Contract DE-AC06-76RLO 1830

PNNL-11668

DISCLAIMER

This report was prepared as an account of work sponsored by an agency of the United States Government. Neither the United States Government nor any agency thereof, nor Battelle Memorial Institute, nor any of their employees, makes any warranty, express or implied, or assumes any legal liability or responsibility for the accuracy, completeness, or usefulness of any information, apparatus, product, or process disclosed, or represents that its use would not infringe privately owned rights. Reference herein to any specific commercial product, process, or service by trade name, trademark, manufacturer, or otherwise does not necessarily constitute or imply its endorsement, recommendation, or favoring by the United States Government or any agency thereof, or Battelle Memorial Institute. The views and opinions of authors expressed herein do not necessarily state or reflect those of the United States Government or any agency thereof.

PACIFIC NORTHWEST NATIONAL LABORATORY
operated by
BATTELLE
for the
UNITED STATES DEPARTMENT OF ENERGY
under Contract DE-AC06-76RLO 1830

Printed in the United States of America

Available to DOE and DOE contractors from the
Office of Scientific and Technical Information, P.O. Box 62, Oak Ridge, TN 37831;
prices available from (615) 576-8401.

Available to the public from the National Technical Information Service,
U.S. Department of Commerce, 5285 Port Royal Rd., Springfield, VA 22161



This document was printed on recycled paper.

**Earthquake-Induced Response
and Potential for Gas Mobilization
in Hanford Waste Tanks**

H. C. Reid
J. E. Deibler

September 1997

Prepared for
the U.S. Department of Energy
under Contract DE-AC06-76RLO 1830

MASTER

DISTRIBUTION OF THIS DOCUMENT IS UNLIMITED *ph*

Pacific Northwest National Laboratory
Richland, Washington 99352

DISCLAIMER

Portions of this document may be illegible in electronic image products. Images are produced from the best available original document.

Summary

Seismic events postulated to occur at Hanford are predicted to cause yielding of the various waste materials in double- and single-shell tanks such that some or most of the waste is driven to completely plastic behavior. The seismic analyses documented in this report evaluated waste response to a 1,000-year design basis earthquake (DBE) event. The three-dimensional finite element computational structural analysis models were used with an assumed nonlinear elastic-plastic material definition. Four waste configurations are analyzed:

- Homogeneous solid
- Liquid-over-solid
- Floating solid-over-liquid
- Floating solid-over-liquid-over-solid.

The homogeneous solid model waste configuration was studied parametrically using two values of shear strength, 300 and 6,000 Pa, and two waste depths, 150 and 300 inches. The two-tier, liquid-over-solid configuration used the same two shear strengths with depths of 300 and 400 inches. Two other models based on a particular tank configuration were evaluated with one shear strength and waste height. The solid-over-liquid waste model approximated the configuration of Tank A-101 assuming a 300-Pa shear strength in the solids layer. The floating solid-over liquid-over-solid waste model represented AN-103 and used a 200-Pa shear strength.

Two gas mobilization criteria were developed based on induced solid mechanics strain conditions. The first is a simple strain threshold, beyond which the solid is assumed "fluidized" and gas bubbles might be released. The second is a derived strain energy density limit. While the first (strain limit) was assigned a single value based on rheological test data, the second varies based on the assumed shear strength of the solid. No detailed gas release model is applied to mobilized solids; gas is assumed to be released from the volume of material in which the limits is exceeded. Based on studies of gas release events in double-shell tanks (Meyer et al. 1997) about 50% of the retained gas in the mobilized region could be expected to exit.

Both the gas mobilization and release criteria are based on shear strain. During the waste response simulations, all models showed harmonic hydrostatic pressures substantially greater than the shear stresses associated with shear strain limit criteria. The lack of definitive data for gas mobilization based on relative contributions between deviatoric (shear) and dilational (hydrostatic) stresses and strains makes it virtually impossible to determine the significance of the pressure waves on gas release. For this reason, potential gas mobilization due to hydrostatic pressure waves was not considered in this study.

The potential effect of high hydrostatic stresses would be to increase gas release if the hydrostatic pressure waves are effective in yielding the waste and mobilizing the gas. Gas mobilization mechanisms can be postulated in which hydrostatic stresses induce cyclic bubble expansion and contraction that could yield the surrounding waste. Most engineering materials do not fail (yield) due to hydrostatic stresses; however, some peripheral evidence is shown that suggests some gas-containing waste does yield due to bubble expansion (hydrostatic pressure decrease) at hydrostatic pressure changes from 1 to 10 times the material's shear strength.

The fraction of the solids volume mobilized based on the various structural analyses and the two mobilization criteria are presented in Tables S.1 and S.2. Table S.1 shows the results of the shear strain limit criterion, and Table S.2 is based on the strain energy density limit criterion.

To identify a particular tank waste condition in the tables, a shorthand notation is used. The particular waste shear strength is denoted by the letters "SS" preceded by the value used. The depth is tabulated as either "Hi" or "Lo" depending on whether the results represent the high or low waste level condition for that configuration. The estimates of potential gas release are greater under the strain energy density criterion than those based on the simple strain limit. The analyses of the solid-over-liquid waste required a material definition of the liquid that was less rigorous than the pure hydro-fluid model that was employed in the other models. The results therefore are not considered conservative, and the potential gas mobilization is believed to be greater than the numbers given (so the use of ">"). A blank entry indicates the case was not analyzed.

Large plastic strains were predicted to occur in all solid waste configurations but were especially violent when a liquid layer was present. This liquid acted as a harmonic oscillator, exacerbating the motion in any contiguous solid layer whether above or below the liquid. This resulted in most of the solids volume exceeding the strain and strain energy limits in configurations 2, 3, and 4, indicating the probable release of a large fraction (~50%) of the retained gas in the 1,000-year DBE studied. This remains consistent with the qualitative estimates given by Stewart et al. (1996) based on spectral analysis.

The analyses also predicted that large wave motion would occur at the surface of the solid material in the homogeneous case even without liquid present. However, these waves were more localized in the central region of the tank and dissipated a large amount of energy. This reduced the

Table S.1. Fraction of Solids Volume Exceeding Strain Limit

Parameter Set	Waste Configuration			
	Homogeneous	Liquid-on-Solid	Solid-on-Liquid	Solid-on-Liquid-on-Solid
300 Pa SS - Hi Depth	0.5%	85%		
300 Pa SS - Lo Depth	~0 %	37%		
6,000 Pa SS - Hi Depth	~0 %	~0 %		
6,000 Pa SS - Lo Depth	~0 %	~0 %		
Tank A-101			> 42%	
Tank AN-103				86%

Table S.2. Fraction of Solids Volume Exceeding Strain Energy Density Limit

Parameter Set	Waste Configuration			
	Homogeneous	Liquid-on-Solid	Solid-on-Liquid	Solid-on-Liquid-on-Solid
300 Pa SS - Hi Depth	5.2%	98%		
300 Pa SS - Lo Depth	12.8 %	80%		
6,000 Pa SS - Hi Depth	~0 %	~0 %		
6,000 Pa SS - Lo Depth	~0 %	~0 %		
Tank A-101			> 68%	
Tank AN-103				99%

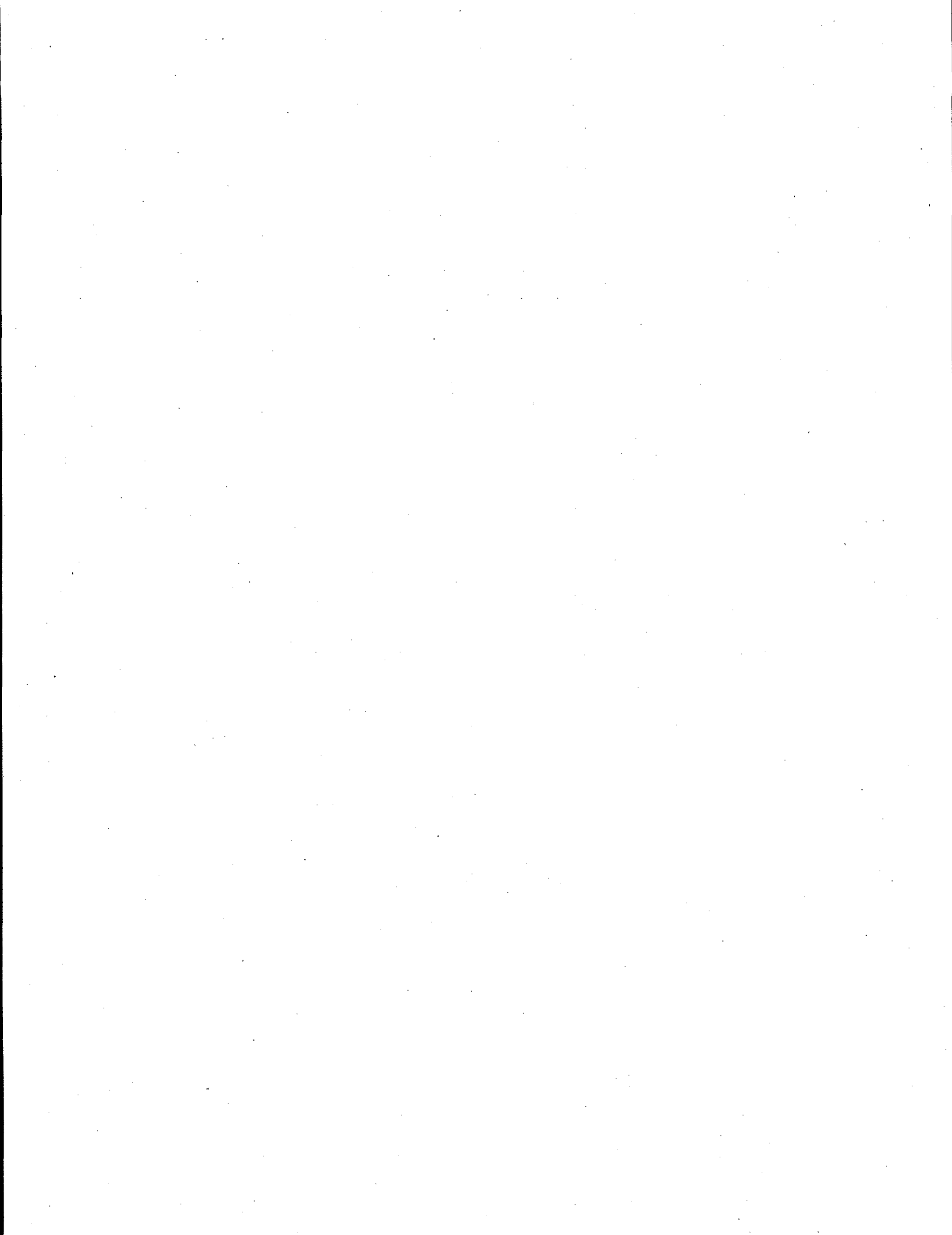
peak stresses and strains elsewhere in the tank. Thus the waste response was much less severe than that predicted by the earlier frequency analyses. Overall gas release fractions of 5–10% would be appropriate estimates for a tank without a significant free liquid layer for a 1,000-year DBE.

At this point, no quantitative estimates can be made of the effect of stronger or milder earthquakes. A 10,000-year earthquake would undoubtedly mobilize a larger fraction of a tank with homogeneous waste, but the release fraction of the other configurations would probably not be significantly greater than 50%. A 100-year DBE might release no gas from a homogeneous tank, but it is not obvious whether the other configurations would release much less gas than the 1,000-year case.

References

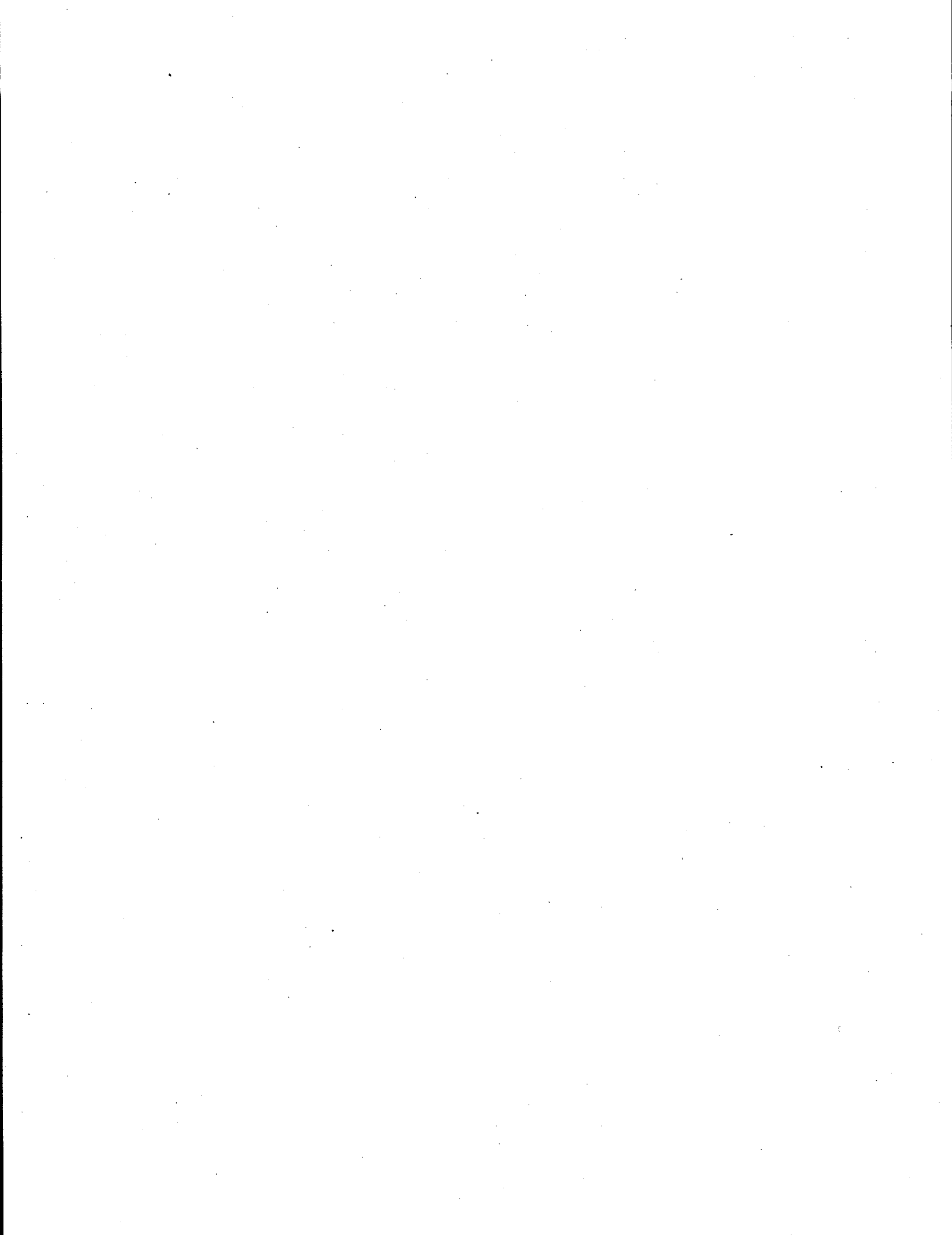
Meyer PA, ME Brewster, SA Bryan, G Chen, LR Pederson, CW Stewart, G Terrones. 1997. *Gas Retention and Release Behavior in Hanford Double-Shell Tanks*. PNNL-11536, Pacific Northwest National Laboratory, Richland, Washington.

Stewart CW, ME Brewster, PA Gauglitz, LA Mahoney, PA Meyer, KP Recknagle, and HC Reid. 1996. *Gas Retention and Release Behavior in Hanford Single-Shell Waste Tanks*. PNNL-11391, Pacific Northwest National Laboratory, Richland, Washington.



Acknowledgments

The authors would like to express their gratitude to C. W. Stewart of PNNL. Without his expertise in blending reviewers' comments on the draft, we would not have succeeded in finalizing this report.



Contents

Summary	iii
Acknowledgments.....	v
1.0 Introduction.....	1.1
2.0 Design Base Earthquake Time History	2.1
3.0 Modeling the Waste Material.....	3.1
4.0 Computational Modeling Methodology.....	4.1
5.0 Waste Configurations and Mechanical Properties.....	5.1
6.0 Gas Mobilization Criteria.....	6.1
7.0 Material Failure Concepts in Structural Analysis.....	7.1
8.0 Results of Seismic Shock on Waste Motion	8.1
8.1 Homogeneous Solid Waste	8.1
8.2 Liquid-over-Solid Waste	8.11
8.3 Solid-over-Liquid Waste	8.21
8.4 Solid-over-Liquid-over-Solid Waste.....	8.26
9.0 Conclusions and Recommendations	9.1
9.1 Summary of Gas Release Extimates.....	9.1
9.2 Conclusions	9.2
9.3 Recommendations	9.3
10.0 References.....	10.1
Appendix: Energy Associated with the Spectrum DBE Event.....	A.1

Figures

2.1	Comparison of the 1992 and Revised DBE Spectra for the Hanford 200 Areas	2.2
3.1	Shear Stress Measurements on Waste Simulants	3.2
4.1	Hanford DBE Acceleration Time History Model (vertical)	4.2
4.2	Hanford DBE Acceleration Time History (horizontal)	4.2
4.3	DBE Displacement Time History Applied with ANSYS (vertical).....	4.3
4.4	DBE Displacement Time History Applied with ANSYS (horizontal)	4.3
4.5	Typical ANSYS 3-D Symmetry Model	4.4
5.1	Configurations Modeled	5.1
6.1	Elastic-Perfectly Plastic Loading and Unloading Hysteresis	6.2
8.1.1	Viscoelastic Model Strain for 150 in., 300 Pa Shear Strength Waste	8.2
8.1.2	Peak Strain Contours for 300 in, 300 Pa Shear Strength Homogeneous Waste	8.3
8.1.3	Peak Strain Distribution for 300 in, 6000 Pa Shear Strength Homogeneous Waste.....	8.4
8.1.4	Time History of Homogeneous Waste Peak Shear Strain	8.4
8.1.5	Time History of Peak Strain Energy Density.....	8.6
8.1.6	Strain Energy Density Distribution for 300 in., 300 Pa Shear Strength Waste.....	8.6
8.1.7	Strain Energy Density Distribution for 300 in., 6,000 Pa Shear Strength Waste	8.7
8.1.8	Time History of Waste Volume Exceeding Shear Strain Energy Density Limit.....	8.8
8.1.9	Time History of Peak Plastic and Total Strain Energy Density.....	8.9
8.1.10	Time History of Peak Plastic Shear and Hydrostatic Stresses.....	8.9
8.1.11	Time History of Peak Plastic and Hydrostatic Strain Energy Densities	8.10
8.1.12	Time History of Hydrostatic Stresses at Three Waste Depths.....	8.11
8.2.1	Time History of Liquid-over-Solid Waste Tank Peak Shear Strain.....	8.13
8.2.2	Peak Strain for 400 in., 300 Pa Shear Strength Waste.....	8.13
8.2.3	Peak Strain for 400 in., 6,000 Pa Shear Strength Waste	8.14
8.2.4	Time History of Volume Exceeding Strain Limit	8.15

8.2.5	Strain Energy Density for 400 in., 300 Pa Shear Strength Waste	8.16
8.2.6	Strain Energy Density for 400 in., 6,000 Pa Shear Strength Waste.....	8.16
8.2.7	Time History of Peak Plastic and Total Strain Energy Density.....	8.17
8.2.8	Time History of Peak Total Strain Energy Density	8.18
8.2.9	Time History of Peak Strain Energy Density.....	8.18
8.2.10	Time History of Peak Strain Energy Density with Depth	8.19
8.2.11	Time History of Volume Exceeding Strain Energy Density Limit	8.20
8.2.12	Time History of Hydrostatic Stresses at Two Tank Waste Depths	8.21
8.3.1	Time History of Peak Shear Strain	8.23
8.3.2	Peak Strain.....	8.23
8.3.3	Peak Strain Energy Density.....	8.24
8.3.4	Time History of Waste Peak Strain Energy Density.....	8.25
8.3.5	Time History of Volume Exceeding Strain Limit Criterion	8.25
8.3.6	Time History of Peak Total and Plastic Strain Energy Density.....	8.26
8.4.1	Time History of Peak Shear Strain	8.28
8.4.2	Time History of Peak Strain Energy Density.....	8.28
8.4.3	Time History of Volume Exceeding Strain Limit and Strain Energy Limit	8.29

Tables

S.1	Fraction of Solids Volume Exceeding Strain Limit	iv
S.2	Fraction of Solids Volume Exceeding Strain Energy Density Limit	iv
8.1.1	Material Properties of Homogeneous Solid Waste.....	8.1
8.1.2	Summary of Results for Homogeneous Waste Configuration	8.5
8.1.3	Peak Plastic Strain Energy Density	8.7
8.2.1	Material Properties of the Solids in Liquid-over-Solid Waste	8.12
8.2.2	Peak Strain and Volume Exceeding Strain Limit Criterion.....	8.15
8.2.3	Maximum Plastic Strain Energy Density	8.20
8.3.1	Material Properties of Solid-over-Liquid Waste.....	8.22
8.4.1	Material Properties of Solid-over-Liquid-over-Solid Waste	8.27
9.1	Summary of Fraction of Solids Volume Mobilized Based on SEDL.....	9.1

1.0 Introduction

In this report the potential for gas release in waste tanks during the earthquakes postulated for Hanford is analyzed. The effect of earthquakes on structures is due to shock and vibration; the actual events that produce the shock are time-varying displacements of the ground surrounding the structures. Analytical methods for evaluating postulated earthquakes rely on time-independent shock "spectra" or, alternatively, time-dependent simulations of actual displacements and forces. Shock spectra techniques are time-independent; the loads are converted to frequency-dependent displacements, velocities, or accelerations that emulate the time history shock. The Newmark-Hall method (Newmark and Hall 1978) is based on frequency spectra and is widely employed in earthquake analyses. Time-independent methods such as Newmark-Hall assume that the induced motion is harmonic and that the vibrations that occur involve only linear elastic strains. This is due to the requirement that "modes" (natural frequencies) of the structure are excited by the earthquake shock spectra. Therefore, a corollary of spectral analysis is modal analysis, and the entire concept of modes involves linear elastic assumptions

Previous evaluations of earthquake-induced gas release from Hanford waste tanks used a shock spectra approach (Stewart et al. 1996). This analysis attempted to predict induced stresses in the waste assuming that the motion could be characterized only by linear elastic stress-strain conditions. The analysis was aimed primarily at determining whether lower-mode excitation could produce stresses and absorbed energy exceeding the elastic limit. The linear analysis predicted a fairly uniform amount of energy absorbed, about 486 to 973 N-m/m³ (~10 to 20 ft-lb/ft³) independent of waste height. The first mode (natural frequency) fell with increased waste height, causing larger strains for a given load. However, the frequency range fell into the spectra where load decreased with decreasing frequency. The overall result was that the effects approximately canceled to give a largely invariant absorbed energy with waste depth. The results did confirm that, indeed, strains beyond the elastic limit were possible and large plastic deformation could be expected. However, since gas release from waste is expected to require large plastic deformation, the use of modal analysis methods assuming only elastic response was not completely appropriate.

Based on this conclusion, a more detailed investigation was undertaken to characterize the behavior of waste when the excitation induces large plastic strains. By its very nature, plastic deformation analysis precludes a frequency spectra approach and requires a time history evolution. Analyses were performed using the ANSYS structural analysis program to predict stress, strain, and energy for various waste configurations. These configurations include solids and liquid layer combinations and variation in waste depth.

The design basis earthquake (DBE) is a postulated 1,000-year event with the appropriate time histories taken from Hanford earthquake evaluation documents. Since there are some differences between recent and older Hanford DBE documentation, an acceptable basis for defining the appropriate time histories is outlined in Section 2.

The seismic structural analyses are performed to determine basic mechanical stress, strain, and energy induced in the waste during the DBE event. Retained gas mobilization criteria are established to interpret the basic mechanical results and estimate the solids volume that is mobilized. These potential gas mobilization and release conditions do not consider the details of gas bubble migration through the waste to the head space. The prediction of transport of the mobilized gas bubbles is not practical within the present analytical procedures. Rather, we assume that significant gas release is probable from the region of solid waste that is mobilized.

The ANSYS structural analyses were performed in English engineering system (ES) units. Graphic presentations of results from these analyses use ES units although the remaining portions of the report use metric units (SI). The waste depth, however, is given in inches when describing a particular configuration. The other ES units from the ANSYS graphic post processing are stress and strain energy density. Stress is given in psi and strain energy density in in.-lb/in.³. For stress, the SI equivalent of one psi is 6894.8 N/m². Strain energy density is energy per unit of volume, so the equivalent of one in.-lb/in.³ is 6894.8 N-m/m³.

2.0 Design Basis Earthquake Time History

This section lays the groundwork for using the time history shock curves defined in *Design Basis Earthquake Time Histories for 1992 SDC-4.1, Rev. 12* (Weiner and Rohay 1992), a Westinghouse Hanford Company document on DBE that develops equivalent time histories for representative spectrum shock conditions at Hanford. A newer document, yet to be released, does not include as much detail.^(a) Our evaluation of seismic induced gas release event (GRE) potential, which treats the waste as an elastic-plastic material, requires the time history models. Resources required to generate such time histories were beyond the scope of this seismic study on gas release potential of waste in tanks, so the displacement time histories have been taken from Weiner and Rohay (1992).

Weiner and Rohay generated three statistically independent time histories that fit the specified Newmark-Hall response spectrum. The Hanford Site response spectra are currently being revised, and time histories have not been generated for the new spectra but are based on the spectrum curves.^(a) The earlier time histories do not match the new spectra, but the characteristics of the waste response and the method of applying the time history loads provide a conservative bias to our analysis.

The 1992 and the new DBE spectrum shock curves for the Hanford 200 area are compared in Figure 2.1. The control point (value at 100 Hz) of the new spectrum is at 0.18 g and is at a lower acceleration than the 1992 Standard Design Criteria (SDC) curve (DOE 1994). The curves diverge at about 0.45 Hz, and the old curve is slightly higher until they cross again at about 10 Hz. A modal analysis of the model being used for the waste seismic analysis revealed 28 frequencies below 0.25 Hz and all of the first 100 modes at less than 0.45 Hz. We assume the tanks will respond at frequencies where the SDC curve specifies a higher acceleration than the new response curves, which provides the conservatism to the analysis.

Additional conservatism is provided by using the full magnitude of the displacement time history in the vertical direction. Typical elastic analyses consider the vertical response spectrum to be only two-thirds of the horizontal spectrum. Also, the model is conservative in ignoring soil-structure interaction. DOE-STD-1020, *Natural Phenomena Hazards Design and Evaluation Criteria for DOE Facilities* (DOE 1994, Section C.4.3), states that the reduction in foundation motion due to soil-structure interaction "increases with foundation plan dimensions and increasing embedment depth."

The philosophy behind the DOE standard is to ensure that DOE facilities protect workers, the public, and the environment from the impacts of natural phenomena hazards. Consequently, conservatisms are built in to earthquake response spectra (DOE 1994, Appendix C). This concept is clearly seen in *Engineering Design and Evaluation*,^(a) in which the evaluation of existing facilities is discussed. The response spectrum curves in that document are constructed with the goal of evaluating buildings, not evaluating an actual earthquake, and so contain built-in conservative modeling.

(a) HNF-PRO-97 Rev. 0, *Engineering Design and Evaluation*, effective October 1997. Lockheed Martin Services Inc., Richland, Washington.

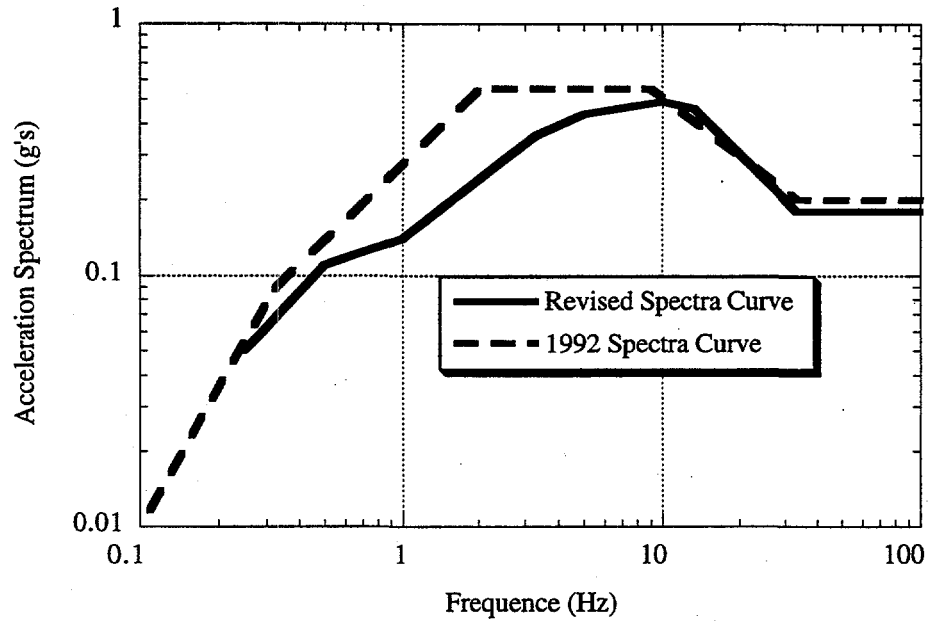


Figure 2.1. Comparison of 1992 and Revised DBE Spectra for the Hanford 200 Areas

3.0 Modeling the Waste Material

The mechanics of solids or solids-like materials are characterized by strain-induced stresses. In fluids or fluid-like materials, stresses are induced by the strain rate (velocity gradients). In solids, the stress-strain relationship is approximately linear and conservative (elastic) until the material yields. During the application of forces (loading), the material can undergo elastic strain and recover to zero stresses when the strain returns to zero. The material may or may not be incompressible. The indication of the compressibility of the material is linked to Poisson's ratio of the material. Poisson's ratio specifies the degree of lateral strain compared to longitudinal strain (or the direction of applied load). A ratio of 0.5 signifies an incompressible material.

While most engineering materials have Poisson ratios of 0.33 to 0.25, liquids or liquid-type materials typically approach 0.5, since they are relatively incompressible. Materials that are hydrodynamic in nature but still exhibit solid mechanics strain-induced stresses typically will behave as nearly incompressible materials. Truly incompressible materials exhibit zero resolved effective stresses since the dilatational portion of the strain tensor reduces to only the hydrostatic pressure. An important consequence of such near incompressible materials is that they necessarily have small shear and Young's moduli because of the relationship between Lamé's constants and the material bulk and Young's moduli (Hughes and Gaylord 1964). Young's modulus, E , is related to the bulk modulus, K , as

$$E = 3(1 - 2\mu) K \quad (3.1)$$

where μ is Poisson's ratio. The shear modulus, G , is related to the Young's elasticity modulus and the bulk modulus as

$$G = \frac{E}{2(1 + 2\mu)} = \frac{3(1 - 2\mu)K}{2(1 + 2\mu)} \quad (3.2)$$

From Eq. (3.2) it can be seen that the bulk modulus becomes very large as the Poisson ratio approaches $1/2$ for a given shear or Young's modulus.

Beyond the elastic limit, after yielding, solids exhibit some form of plastic deformation characterized by a permanent strain when the applied forces are removed. The actual mechanism by which the material yields and the process by which it unloads (i.e., returns to finite strain at zero stress) can be quite complicated. Many hardening models have been developed to characterize the physical response of different materials including kinematic hardening, isotropic hardening, the Drucker-Prager frictional model, and simple nonlinear elastic behavior. The kinematic and isotropic hardening models apply to metals, while nonlinear elastic behavior is more suitable for hyperelastic materials such as rubbers and polymers. The Drucker-Prager model is applicable to granular soil structures (Zienkiewicz et al. 1975). Other stress-strain relationships may assume hardening plastic or perfectly plastic assumptions. The material unloading can be an arbitrary stress-strain curve.

Initially, the Drucker-Prager model was employed for the solid mechanics modeling of the response of tank waste to an earthquake. After numerical difficulties were encountered, an elastic perfectly plastic model was used. The assumptions made in this model are that the stress-strain

curve is linearly elastic to the yield point and behaves as a perfect plastic following yielding. This follows some simulant experimental data reasonably well. The ultimate strain for waste material to fluidize (where gas bubble release can occur) can be in the range of 100% strain (Whitney et al. 1996).

The material properties are based on data from waste simulant tests.^(a) These tests indicated typically low shear moduli (100's of Pa) along with linear elastic limit strains (yield strain point) in the 5 to 10% range (Figure 3.1). Extremely stiff waste or "hard pan" can have shear strengths that are in the kPa range. Simulant waste studies (Gauglitz et al. 1995) measured shear strengths with magnitudes of 2 kPa for bentonite solutions to 8 kPa for glass beads. The highest shear strength measured on real waste is in the 6 to 10 kPa range.^(b) For purposes of this study, an upper limit of 6 kPa shear strength is used. In-situ ball rheometer data from double-shell tanks (DSTs) (Meyer et al. 1997) indicate yield stress on the order of 100–200 Pa. The lower value of shear strength is therefore set at 300 Pa.

Because of the nature of the waste, large strains are possible before it becomes fluid enough to release trapped gas. It is apparent from the proposed material model that very large strains are to be considered in the seismic analyses. Modeling of materials that undergo large displacements requires nonlinear geometric analytical capability. The ANSYS finite element program incorporates such large deformation analysis capabilities with compatible elements and can be used for the seismic analyses.

Substantial plastic strain during an earthquake is likely since the elastic moduli and yield strain of the tank waste material are small. For elastic deformation, the material may undergo combinations of tensile and compressive strain along with distortion. This results in tensile, compressive, and shear stresses. When the material becomes plastic, it converts into an incompressible form such that no volumetric change may occur—only distortion can occur. For this reason, all plastic strain results from combined shear strains. Likewise, all plastic strain energy density results from the combined shear strain energy densities.

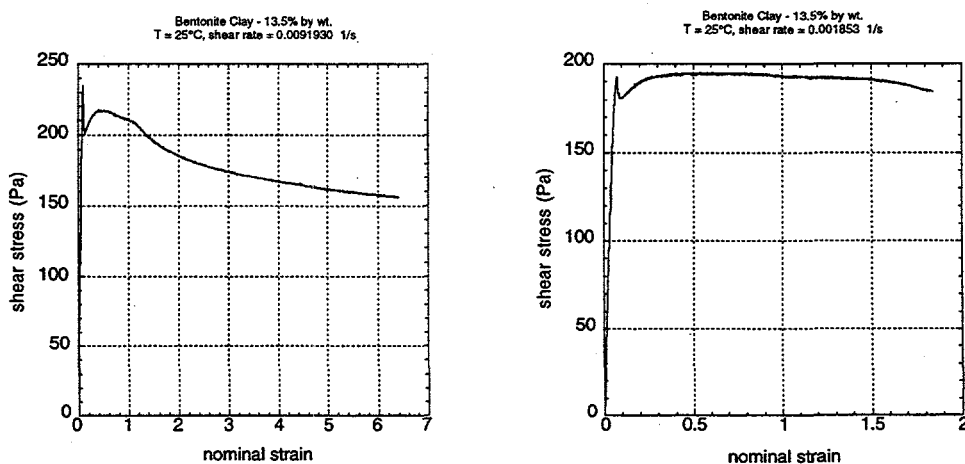


Figure 3.1. Shear Stress Measurements on Waste Simulants

- (a) Phillips JR. May 1994. "A Basic Rheological Survey of Simulant Materials for the Ball Rheometry Project." Letter report, PNNL, Richland, Washington.
 (b) Personal communication with PA Gauglitz (PNNL) on waste yield strength derived from videos of waste extrusion.

Stress is typically characterized as "true" or "engineering." From a one-dimensional point of view, engineering stress is defined as the load in the member divided by the initial cross-sectional area. By the very definition of Poisson's ratio, the strain induced in the direction of the load results in lateral strain that actually alters the effective cross-sectional area of the load. The stress obtained by dividing the load by the actual area is the "true" stress. Although somewhat more complicated, the same applies to shear stresses. In most engineering analyses, where the strain is small the difference is negligible. However, for very large deformation where strains can reach several hundred percent, the difference is important.

The difference between engineering strain and true strain also becomes important in determining property data from experiments. It is fair to say that using rheometers to measure shear stress versus strain in regions of very large strains actually results in some type of pseudo-strain being measured. These data must be converted into property data useful for analysis. Without a clearer understanding of the solid mechanics nature of the various waste materials, it is assumed that the simulant data on stress-strain, such as that shown in Figure 3.1, is actually "true" strain data. This is a practical compromise, realizing that the uncertainty in actual waste properties exceeds the difference between the true and engineering values.

4.0 Computational Modeling Methodology

The structural analysis computer program ANSYS (Kohnke 1994) was employed to simulate seismically induced motion in several waste configurations. ANSYS is a finite element model intended for static and transient structural analyses. Based on mechanical energy conservation laws, strains can be predicted for given applied loads at discrete nodal points that represent a mathematical model of the geometry. Material property data, including stress-strain relationships, must be supplied by the user. ANSYS performs large deformation elastic-plastic analyses on a wide class of nonlinear material configurations, including elastic-perfectly plastic behavior.

An ANSYS model is developed from suitable element types (selected from a library in the program) that represent the dimensionality of the problem, material features such as plasticity and incompressibility, and degree of interpolation (called "shape" functions). Appropriate boundaries and boundary conditions, along with restraints and initial conditions, must also be specified.

Of prime importance is the model defining the stress tensor in the system of conservation equations. For homogeneous elastic materials, Hooke's law is an appropriate formulation for the stress tensor. For more complex conditions such as anisotropic properties, plastic deformation, and hyperelastic or viscoelastic tensile behavior, different stress tensor formulations are derived. These formulations are available to the structural analyst as an array of "element types" and are typically identified by a combination of three features: 1) the dimensionality of the model (i.e., 1-D, 2-D, or 3-D), 2) the interpolation basis of the finite element (roughly the degree of polynomial approximation of the assumed spatial variation of strain across the element), and 3) the material stress tensor model.

From current studies on waste and simulant testing, it is apparent that very little is actually known about the solid mechanics constituent stress laws of these materials. In the seismic analyses, several element types were used in the preliminary stages to evaluate the effects of stress tensor formulation on resulting deformation. Otherwise, all of the element types were three-dimensional and used a linear (trilinear) basis. One was a hyperelastic element type (ANSYS Hyper86 type), one a viscoelastic element type (ANSYS Visco107 type), and one an isoparametric solid (ANSYS Iso45). The elements are described in the ANSYS Theory Manual (Kohnke 1994).

The isoparametric solid element type is the most commonly used element in ANSYS and supports orthotropic elastic-plastic stress tensor modeling. Various elastic yielding models are available, but the classic von Mises maximum distortion energy criterion was assumed applicable. The hyperelastic element type is actually a nonlinear elastic stress tensor formulation that models large deformation assuming that the material never plasticizes. The element supports the Mooney-Rivlin material constitutive law, which is appropriate for nearly incompressible natural rubbers. The viscoelastic element type is a rate-sensitive material model with elastic-plastic behavior.

The seismic time histories representing a 1,000 year DBE are taken from Weiner and Rohay's (1992) Hanford DBE document (Figures 1-1 and 1-2). These time histories are of artificial events that will reproduce the appropriate shock spectra. The DBE has a 23-second life, including a 3-second ramp-up and 3-second ramp-down. This has the effect of containing the maximum acceleration amplitude to the period between 3 seconds and 20 seconds. The tank models were symmetric through one vertical plane, so two orthogonal boundary conditions could be applied. The vertical and horizontal accelerations, taken from the DBE document, are presented in Figures 4.1 and 4.2, respectively. The equivalent displacement histories (Figures 3-1 and 3-2 in Weiner and Rohay 1992) are shown in Figures 4.3 and 4.4.

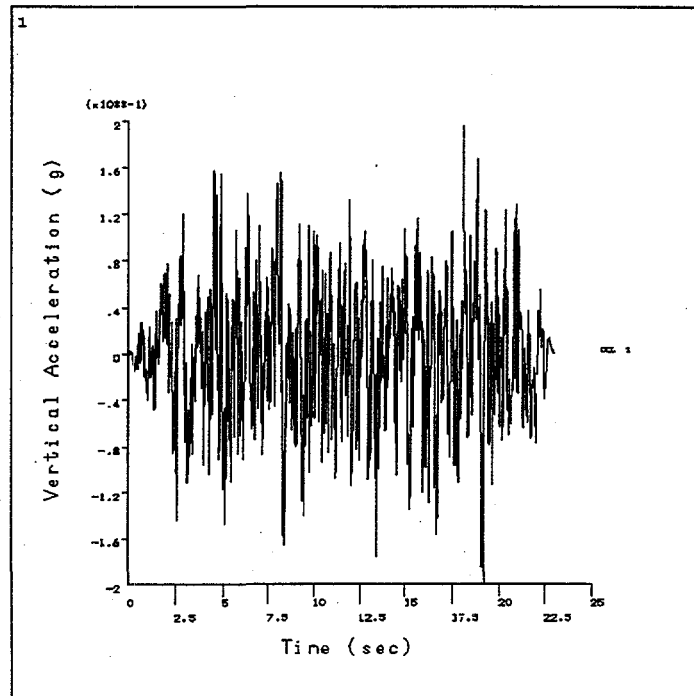


Figure 4.1. Hanford DBE Acceleration Time History Model (vertical)

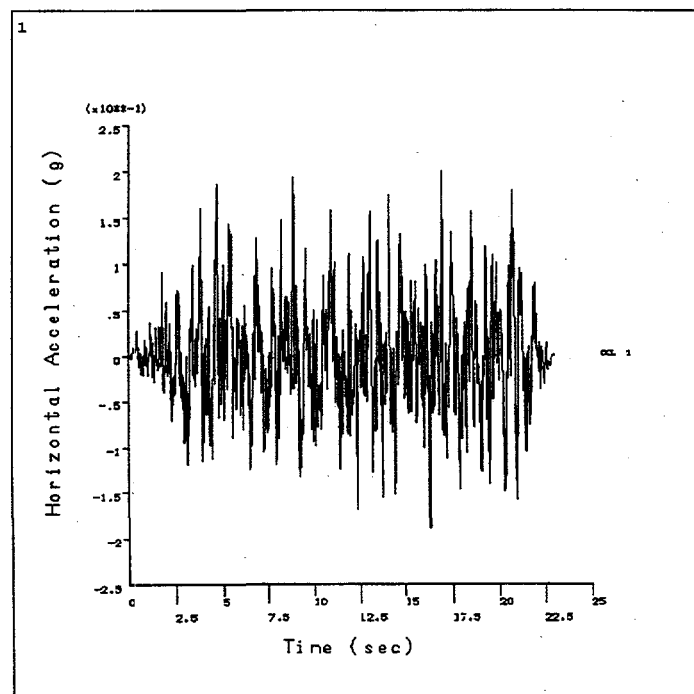


Figure 4.2. Hanford DBE Acceleration Time History (horizontal)

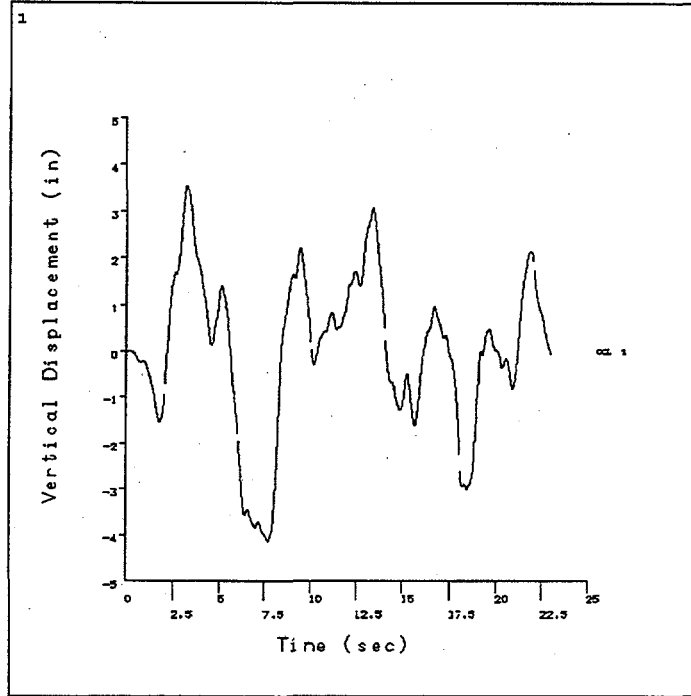


Figure 4.3. DBE Displacement Time History Applied with ANSYS (vertical)

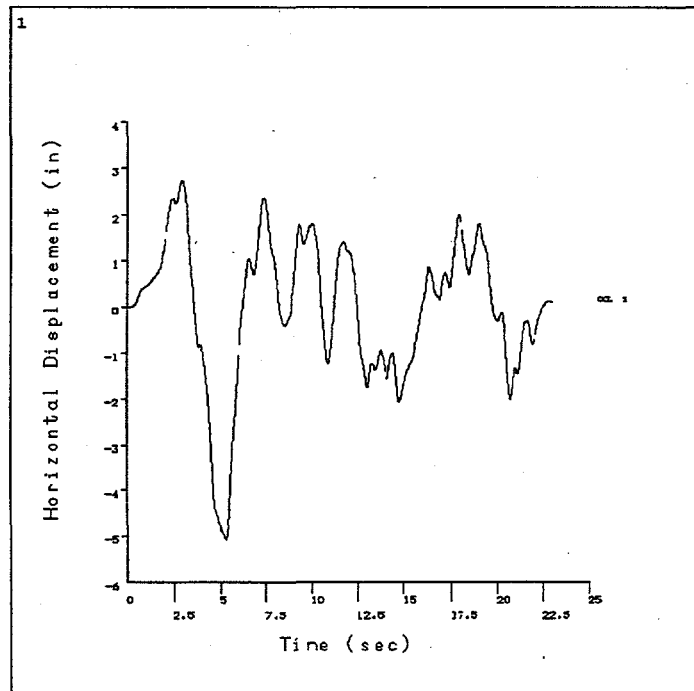


Figure 4.4. DBE Displacement Time History Applied with ANSYS (horizontal)

The solid waste was modeled using the ANSYS three-dimensional element with large deformation elastic-plastic capability. Where practical, liquids (in liquid-solid waste configurations) were modeled with an incompressible element (ANSYS fluid element FLUID80) exhibiting only hydrostatic stresses and transmitting no shear stresses. In cases in which numerical difficulties were encountered, the liquids were modeled as special cases of solid materials. This was accomplished using the 3-D isoparametric element type and specifying a high bulk modulus along with a very low shear modulus.

Figure 4.5 shows the half-symmetry model of the waste. Each model simulates a tank 75 ft (22.86 m) in diameter with the waste depth set according to the configuration being simulated. The outer boundary was assumed to be the floor and walls, so loads were applied directly to the waste boundaries. Note that this conservatively ignores the decoupling inherent in the DST annulus structure. The surface of the waste was assumed to be a free surface, and no loads were applied on it. Based on U.S. Nuclear Regulatory Commission (NRC) approved procedures, two orthogonal time dependent loads were applied simultaneously. The principal component was assumed to be 100% of the 1992 DBE vertical displacement (Figure 4.3), and the other orthogonal component was 100% of the 1992 DBE horizontal displacement (Figure 4.4).

The time step in transient simulations must be appreciably smaller than the Courant limit, or the time for a pressure wave to transverse the typical nodal spacing. The typical acoustical velocity in a liquid with a 5% gas fraction is 50–60 m/s. The typical nodal spacing in the seismic models is around 2 meters, so the Courant limit is about 0.03 second. The analyses used a fixed time step of 0.005 second over the 23-second DBE seismic event (~5,000 steps), which allowed the solution to converge with a nominal number of iterations. ANSYS typically can handle plastic strains as large as several hundred percent, but convergence becomes increasingly difficult and smaller time steps are automatically applied.

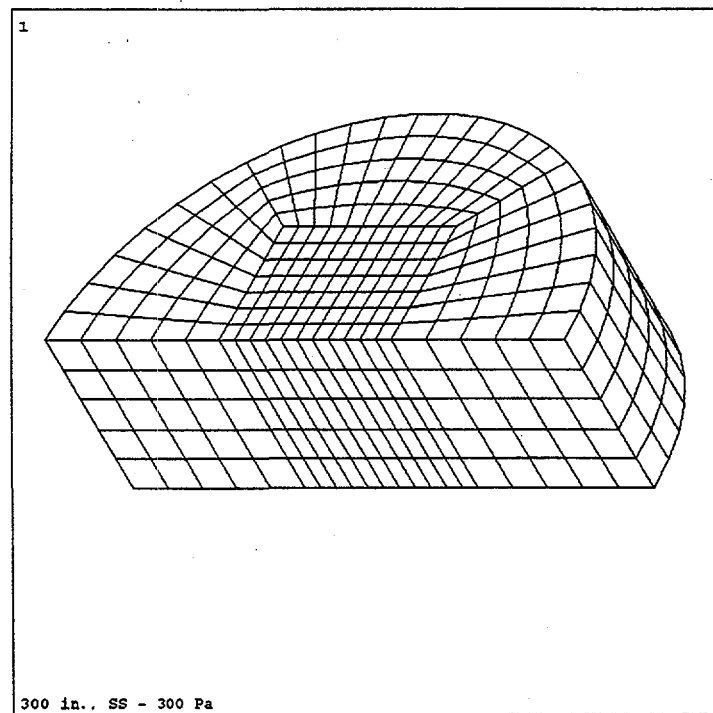


Figure 4.5. Typical ANSYS 3-D Symmetry Model (homogeneous, 300 in. depth)

In some of the simulations, large plastic strains caused convergence difficulties and/or inordinately small time steps. These models were closely inspected for the cause and degree of localized severe deformation and material damping was introduced reduce the computational difficulties. Further details concerning the approach to stabilize large deformation plastic strain analyses are discussed in Section 8.

5.0 Waste Configurations and Mechanical Properties

Since the waste configuration for DSTs and single shell tanks (SSTs), including material composition and waste levels, is unique to every tank, a small group of typical tank configurations was developed for analysis purposes. Four types of generic tanks were identified: one with homogeneous solid waste throughout, a second with a liquid layer over the solid sludge, the third with a solids layer over the liquid, and the fourth with a liquids-over-solid configuration with a solid crust. Figure 5.1 exhibits these four types of tanks.

In the analyses of waste in tanks, the tank shell and wall are considered rigid restraints. DBE time-dependent loads are applied to these boundaries. The top surface of the waste is a free surface. Only the solid portions of a waste for any particular configuration are assumed to contain gas. The solid, liquid, and crust are treated as continuum material, so no gaps or voids (cavitation) can occur.

For each waste configuration, parametric analyses are performed on sludge material properties and waste height. A constant value of 5% was employed for the elastic strain limit for the solids in generic configurations. The homogeneous solid and liquid-over-solid tank models assume densities of $1,700 \text{ kg/m}^3$ for the waste and $1,000 \text{ kg/m}^3$ for the liquid. Also, two different shear strengths, 300 and 6,000 Pa, are considered for solids. The remaining two waste configurations use various material properties that are based on particular Hanford tanks and are

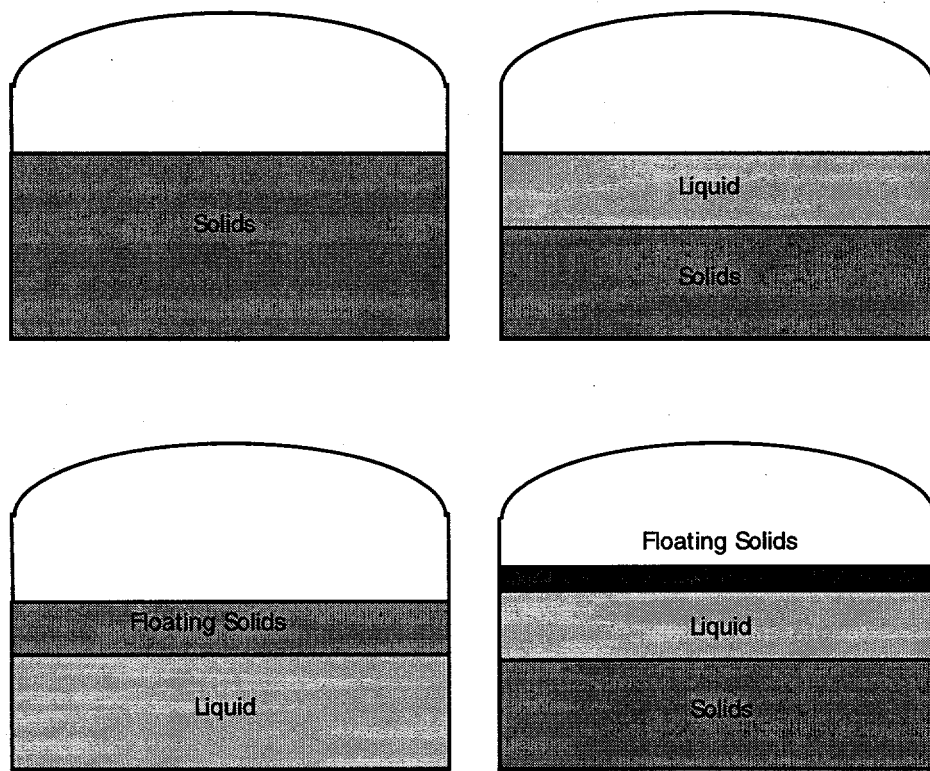


Figure 5.1. Waste Configurations Modeled

discussed later. The elastic strain limit and shear properties then were used to calculate the shear modulus from

$$G = \frac{\tau_y}{\epsilon_y} \quad (5.1)$$

where τ_y is the elastic yield shear stress, and ϵ_y is the elastic strain limit. The bulk modulus is obtained by using the idea that bulk modulus is related to the acoustical velocity of the medium (Avallone and Baumeister 1987) by

$$K = \rho c^2 \quad (5.2)$$

where K is the bulk modulus, c the acoustical velocity, and ρ the bulk density of the medium.

Based on the classic approximation of gas bubbles in liquid media, the acoustical velocity can be expressed as (Stewart et al. 1994)

$$c^2 = \frac{kp_0}{\rho_l \alpha(1-\alpha)} \quad (5.3)$$

where p_0 is the local static pressure, k is the polytropic constant for bubble compression or expansion, α is the gas volume fraction, and ρ_l is the liquid density. This acoustic velocity expression assumes the non-gas solids are all incompressible liquid. In fact, using different densities in Eq. 5.2 and 5.3 (bulk and liquid) is probably not consistent because the derivation of a uniform waste bulk modulus would involve an effective density. For this reason, they are assumed to collapse to the identical value so they effectively cancel each other.

From the relationships above, it is apparent that the bulk modulus is primarily dependent on gas volume content and the depth of the tank. The depth enters the relationship because the local pressure is taken as the local hydrostatic pressure at the average waste depth. Of course, if the bulk modulus coupling with local hydrostatic pressure were rigorously followed, the modulus would vary with distance through the waste. This is not practical with the present finite element analysis model, and the error associated with the depth variation is about $\pm 15\%$ of the nominal value. This is within the uncertainty of the material modulus for a given pressure.

Young's modulus, which is the elastic tensile stress per strain slope, can be related to the bulk and shear moduli as

$$E = \frac{9KG}{3K - G} \quad (5.4)$$

and Poisson's ratio can be derived from

$$\mu = \frac{3K - 2G}{6K + 2G} \quad (5.5)$$

Using typical properties for waste material, $1,700 \text{ kg/m}^3$ for the bulk density, 5% gas volume fraction, and $1,000 \text{ kg/kg/m}^3$ for the liquid density, the bulk modulus is estimated to average about 3.55 MPa ($\sim 500 \text{ psi}$). The shear modulus for 300 Pa shear strength material would be 6 kPa and 120 kPa for a 6 kPa strength material. Poisson's ratio depends on shear strength and bulk modulus. Since the bulk modulus is dependent upon local pressure (Eq. 5.2 and 5.3), for

300 Pa shear strength material 300 in. deep with a solids density of $1,700 \text{ kg/kg/m}^3$, Poisson's ratio would be about 0.499. It would decrease to 0.479 for 6 kPa strength material with a 150 in. depth. These results indicate that typical waste material is highly incompressible (μ equal to 0.5 is perfectly incompressible), as would be expected from a heavily liquid-saturated medium.

For the solid-over-liquid tank configuration, Tank A-101 was used as the typical example. The average gas fraction for this tank is about 14% in the nonconvective layer (Shekarriz et al. 1997). Here the bulk modulus computed by Eq. 5.2 is 1.4 MPa. For the liquid-over-solid topped with crust tank configuration, Tank AN-103 was used as the typical example. The average gas void fraction for this tank is about 12% in the nonconvecting layer.

The waste heights were varied as part of the parametric analyses. These sets were assigned based on typical waste height ranges observed in Hanford tanks. For the homogeneous solids tanks, 150 in. (381 cm) and 300 in. (762 cm) overall waste heights were analyzed. For liquid-over-solid configurations, 300 in. (508 cm) and 400 in. (1,016 cm) were used based on typical DST configurations. The total waste height was assumed to be split equally between liquid and solid. Thus for a 300 in. waste depth, 150 in. was liquid and 150 in. was solid. For the solid-over-liquid tank configuration, where Tank A-101 was used as the example, a single overall height of 363 in. (992 cm) was used with the solids layer starting at 196 in. (498 cm) elevation. For the tank model with a floating solids layer, a single waste height was also assumed based on Tank AN-103, which consists of 149 in. (380 cm) of solids, topped by liquid to an overall waste height of 312 in. (792 cm) and capped with a 36 in. (92 cm) thick floating solids layer on top. The shear strength of the solids in Tank A-101 was assumed to be 300 Pa. The shear strength of the solids in Tank AN-103 was assumed to be 200 Pa based on ball rheometer measurements (Meyer et al. 1997).

To introduce some uniformity in material mechanical properties for the analyses, some of the variations in the conditions that influence the properties are averaged and the final property values are reduced to one or two common numbers. For this reason, the variation in bulk modulus, which is related to local pressure and therefore depth, is assigned one value for all tanks in the homogeneous and liquid-over-solid models. Similarly, Poisson's ratio is determined from this assumed single valued bulk modulus and therefore varies only because of shear modulus values assumed. For the solid-over-liquid-over-solid waste and the solid-over-liquid configurations, the properties are modeled directly from a specific tank condition, and no parametrics in waste depth or material mechanical properties are involved.

The liquid in the liquid-over-solid and solid-over-liquid-over-solid models used incompressible fluid features and were modeled with the ANSYS element, FLUID80. This element uses a bulk modulus that was assumed to be the same as that of water (339,000 psi or 2,337 MPa). It also employs a molecular viscosity that comes into play as a damping coefficient. Rheological data show that the supernatant liquid is similar to water and that such low viscosities have no real damping effect for these analyses. The material model effectively makes the supernatant an elastic oscillator with no energy absorption.

For the unique case of solid-over-liquid, the FLUID80 element proved to be numerically unstable, and the computational model failed to obtain converged equilibrium solutions. This appears to be caused by the fact that most of the DBE shock load is applied directly to the liquid, which now lies on the floor as well as against the walls of the tank. This ANSYS fluid element is sensitive to initial mesh distortion, and it appears from close examination that without much greater refinement in the model, an adequate solution is not feasible. The necessary refinements were prohibitive in terms of computational resources so the pure fluid element had to be replaced with a highly incompressible elastic model.

Using a weak elastic solid in place of an incompressible fluid material model introduces some nonconservatism. The elastic solid "fluid" exhibits strain-induced stresses that are not valid for a fluid. These stresses tend to restrain the motion of the "fluid" to a greater degree than pure bulk compressive forces from an incompressible fluid material model. However, a weak elastic solid absorbs no net energy and still transmits similar hydrostatic stresses. While the weak elastic solid is not an optimal representation of an incompressible Newtonian fluid, it is a reasonable approximation for quasistatic, non-Newtonian fluids under load. The most serious discrepancies would occur at large strains (several thousand percent). Since large strains are quite localized, the main effect of the elastic model is also localized. In any case, the large plastic strains predicted by either the incompressible fluid or weak elastic solid "fluid" material exceed the validity of the mechanics in ANSYS.

6.0 Gas Mobilization Criteria

Predicting the response of waste to an earthquake is necessary to predict potential gas release. The mechanisms for waste yielding and gas mobilization are quite complex and involve elastic limit yielding of the binding solid-liquid matrix with finite plastic strain deformation, plastic strain work, and thixotropic thinning processes. For the seismic analyses, two of these mechanisms, total shear strain and plastic work (strain energy density), are postulated and can be calculated by structural analysis methods. The spatial variations of both of these quantities are predicted with evolving time during the structural analysis of the DBE event described above. Gas release here specifically addresses the condition of releasing trapped gas so it can migrate upward. Typically, the gas is expected to migrate all the way to the tank headspace, but the details of this process have not yet been modeled. Therefore, the term "gas mobilization" in this report implies release from the entrapping solids enabling migration. It can be conservatively assumed that all the gas that is mobilized is eventually released to the headspace.

The first criterion for potential gas mobilization and release is based on the energy criterion for gas release by buoyant displacement that is postulated for DSTs (Meyer et al. 1997). This is effectively a total shear strain limit (SL) criterion, and it assumes that gas release results when the elastic plus plastic shear strain exceeds roughly 100%. In the present analyses, plastic strain makes up 95% of this criterion because the assumed elastic yielding occurs at only 5% strain.

For the purposes of this analysis, the total plastic strain is assumed equivalent to shear strain and is used as the gas mobilization strain criterion. Classic plasticity theory assumes that plastic strain only occurs due to deviatoric shear stress and not due to dilatational stress (incompressibility). That is, the material changes shape but it does not change volume. Also, if a material is loaded in pure shear, the equivalent von Mises distortion strain is equal to the applied shear strain. Because a material becomes incompressible when it is plastic, and no resolved effective stresses are introduced, the stresses are all shear.

The second gas release criterion is strain energy density. This criterion assumes that total shear strain energy absorbed by the waste from repeated shear strain correlates to conditions of gas mobilization, as illustrated in Figure 6.1. In simplified form, shear strain energy can be defined for small strains as

$$E = \int \tau A d\delta \quad (6.1)$$

where E is the shear strain energy, τ is the shear stress, A is the surface area to which the shear strain is applied, and δ is the shear displacement. The shear strain energy density is strain energy per unit volume, so

$$e = \frac{E}{\vartheta} = \frac{1}{\vartheta} \int A \tau d\delta = \frac{L}{\vartheta} \int A \tau d\varepsilon \quad (6.2)$$

where ϑ is the volume of the strained material, L is the undeformed length, and ε is the shear strain, δ/L . Since L/ϑ has units of area, the resulting expression has units of $\tau \cdot \varepsilon$ ($\text{N} \cdot \text{m}/\text{m}^3$). Eq. 6.1 also exhibits the "true" strain nature of the strain energy density for which true strain area, A , is accounted. Finally, as with the assumptions made for total strain criteria, the shear strain energy

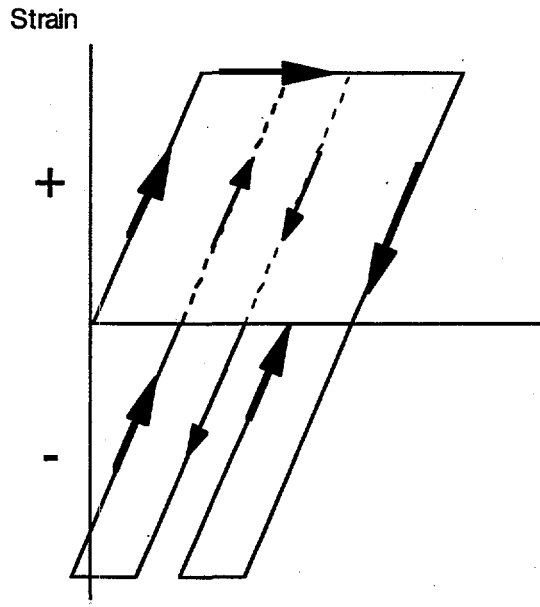


Figure 6.1. Elastic-Perfectly Plastic Loading and Unloading Hysteresis

density is related to plastic strain only. The elastic strain energy does not appear because its path integral is identically zero due to the assumption that the material unloading modulus is the same as the elastic modulus.

The strain energy density limit (SEDL) criterion is not equivalent to the strain limit criterion because of the plastic expansion and compressive strain overlap. Because of the cyclic loading of the waste with large plastic strain, it is possible for a material that never exceeds 100% strain to have strain energy densities several times that of a 100% SEDL.

The shear SEDL for gas release conditions is based on the 100% strain of the first gas release criterion. The maximum shear strain energy density limit for gas release is computed as

$$e_{\max} = \frac{\delta A_0}{\vartheta} \int \tau_y d\epsilon \cong \tau_y \epsilon_{\text{plastic}} \quad (6.3)$$

where τ_y is the shear strength of the material. The approximation involves the cancellation of δA_0 with ϑ under the assumption that no significant change in the original volume occurs due to plastic deformation. This is consistent with the nearly incompressible properties of the waste. Also, the elastic strain energy does not appear because its path integral is identically zero, assuming that the material unloading modulus is the same as the elastic modulus. The values of strain energy density limits are numerically equal to the waste yield stress since the plastic strain is assumed to be 1.0 (100%).

7.0 Material Failure Concepts in Structural Analysis

In the simplest form, the requirements for identifying appropriate material yielding and gas mobilization criteria are in hand. For both the strain limit and SEDL criteria, the magnitude and extent of shear (plastic) strain and/or plastic strain energy density are predicted using the analytical tool ANSYS. However, as part of the basic process of defining an elastic-plastic material model, specific elastic yielding concepts are introduced that have subtle mechanical stress-strain behavior associated with them. In general, most of the "typical" engineering material models that have been developed for elastic-plastic materials, such as isotropic and kinematic hardening models, employ some form of resolved strains to characterize the elastic yield criteria. Elastic-perfectly plastic material models are subsets of these general material classes.

Elastic yielding in solid mechanics is determined by converting predicted stresses into strains. The practicality of the failure methodology, then, is that strain-induced stresses are combined into some form of equivalent effective stresses that are tested against the material yield strengths. Such failure models include the maximum principal stress theory, the maximum shear stress theory, or a maximum energy density theory (such as von Mises stresses). As detailed in Section 6, the present analysis employs both a shear strain and a strain energy density failure model for the potential gas mobilization and release criterion but also assumes a von Mises yielding model. The significant point is that the yielding models are not direct strain models but resolved stress corollaries.

The literature on Hanford waste properties reports shear strength rather than tensile strength. However, tensile strength is more commonly used in describing the yielding of engineering materials. The von Mises yield criterion was used in this analysis to relate shear and tensile yielding behavior. This criterion (also called the maximum distortion-energy theory) is based on experimental data that show yielding in ductile materials is often dominated by shear distortion rather than bulk compression or dilatation (Malvern 1969). Following this theory, the deviatoric (shear) stress tensor can be expressed as

$$S_{ij} = \sigma_{ij} + \delta_{ij}p \quad (7.1)$$

where p is the hydrostatic pressure

$$p = -\frac{\sigma_{ii}}{3} \quad (7.2)$$

Index notation is used here with repeated indexes indicating summation of the three normal stress components. The von Mises equivalent stress is then calculated as

$$\bar{\sigma}_i = \sqrt{\frac{3}{2} S_{ij} S_{ij}} \quad (7.3)$$

For the uniaxial tension test ($\bar{\sigma}_i = \sigma_1, \sigma_2, \sigma_3; \sigma_1 > 0, \sigma_2 = \sigma_3 = 0$), the equivalent stress is equal to the uniaxial stress and the equivalent plastic strain is equal to the uniaxial plastic strain. This allows defining an elastic/plastic stress strain relationship from uniaxial test data that also apply to yielding under biaxial and triaxial stress states. Yielding occurs in a uniaxial tension test when $\sigma_1 = \sigma_y$ and $\sigma_2 = \sigma_3 = 0$. If a specimen is loaded in pure shear, then the same level of equivalent stress occurs when

$$\tau_y = \frac{\sigma_y}{\sqrt{3}}$$

Therefore, if one assumes that the von Mises yield criterion applies, then the tensile yield strength can be estimated by multiplying the shear strength by $\sqrt{3}$. This method was used to estimate the yielding condition under triaxial stress from the shear strength data. (Note: The Tresca yield criterion, commonly used to describe the yielding of brittle materials, estimates the tensile yield strength as two times the shear yield strength. Comparing the shear to tensile strength conversion factors of the Tresca and von Mises criterion shows a difference in the estimated tensile strength of only 15%.)

In themselves, these material models do not necessarily constitute difficulties because the experimental tensile and shear strengths of waste materials tend to follow trends similar to other engineering materials. However, the near incompressibility of the waste has a significant effect on the nature of the material yielding process. Because of the large bulk modulus (compared with the shear modulus) and the highly incompressible nature of the waste solids, dilatational strains (elastic volume changes) can occur that result in large hydrostatic stresses (pressures) with the resulting resolved effective stresses that are almost zero. A yield criterion based on resolved effective stresses (such as von Mises) in a nearly incompressible material allows the hydrostatic pressures to be greater than the effective yield strain without violating the elastic limit yield criterion. As a corollary, hydrostatic stresses much greater than the simple one-dimensional strain limit can be produced without affecting the material elastic limit yielding.

While this may at first sound unreasonable, it becomes clearer when considered in the context of typical material response under tensile and shear forces versus hydrostatic forces. An engineering material such as steel, that is strained, for example, by constraining one face and loading its opposite, can be expected to yield when its resolved effective stresses exceed its elastic limit. However, if the same material is tossed into a deep pool of water where the local hydrostatic pressures are greater than the elastic limit stresses, it would experience large volumetric dilatational changes with no distortion. The principal stresses would be equal to the hydrostatic pressure, but the shear stresses would be zero; therefore, the material would not yield. Typically, then, engineering materials do not fail due to hydrostatic forces.

During the seismic event we would expect to see cyclic dilatational pressure "waves" passing through the tank waste. Note that this hydrostatic stress is related to the elastic portion of the strain only, since during the perfectly plastic dilatation the material is perfectly incompressible. Even so, the 5% elastic strain limit can result in a $K \cdot 3\epsilon$ (bulk modulus times the sum of the three orthogonal elastic strain limits) change in hydrostatic stress, which would be on the order of 0.5 MPa (~75 psi). The dilatational strains would also translate into effective hydrostatic strain energy densities that are much larger than shear strain energies. Therefore, the strain energy component due to bulk compression was subtracted from the total strain energy before comparing it with the strain energy criterion.

It is difficult to prescribe a potential failure criterion for these hydrostatic pressure waves based on contemporary knowledge of waste yielding. One study (Whitney et al. 1996) that has addressed the waste level response to barometric pressure changes found that the level fluctuation data exhibit a classic elastic strain-plastic strain hysteresis. When under load, the waste resists dilatational volume changes in the gas until some point at which the material exceeds what appears to be a yield point. Further loading produces volume changes that follow the simple gas laws for the trapped gas. Since the barometric effects are cyclic, repeated elastic strain and yielding occur with time.

The repeated cyclic yielding has not been identified as an important mechanism for gas release. However, the largest barometric pressure swings that occur during winter storms have apparently triggered measurable gas releases in SSTs (Wilkins et al. 1997). The time scale of a shock hydrostatic pressure wave in a DBE is much shorter than that of a barometric pressure cycle. In addition, a large barometric pressure change represents a few percent of the nominal tank hydrostatic pressure, while the hydrostatic pressure waves in a DBE are expected to be over an order of magnitude higher—roughly half the nominal pressure.

Even after this comparison, it is not clear that hydrostatic pressure waves from the DBE alone can mobilize enough gas for a significant gas release. The more important, but also more difficult, question is whether the cyclic compression and expansion due to dilatational strains are worse than the deviatoric shear strains as a global gas release mechanism.

The present argument derived from barometric pressure response investigations proposes that the dilatational strains primarily are absorbed in the bubbles without gas mobilization. Even though local yielding around the bubble may occur, massive shear yielding is still required for the gas to be mobilized sufficiently to result in a release to the headspace.

In this report, the failure mechanisms that would lead to yielding are assumed to obey the von Mises distortion energy criterion. The material failure criterion that would lead to gas mobilization, are restricted to shear phenomena. However, a discussion of hydrostatic stress-related conditions is presented to provide trends and comparisons with shear-related phenomena.

8.0 Results of Seismic Shock on Waste Motion

The motion that results from the DBE may be qualitatively summarized in terms of the stiffness of the waste tank configuration. The stiffness may be characterized as similar to the stiffness of a spring under harmonic excitation. This stiffness can be viewed from the perspective of a simple beam rigidly fixed at one end and shaken laterally. The beam stiffness, K , is related to the beam geometry and material modulus, E , as

$$K \propto \sqrt{\frac{E}{L^2}} \quad (8.1)$$

where L is the length of the beam. For the waste tank, the beam length is converted into the depth of the waste. It is apparent, then, that a stiff waste is one in which the modulus divided by the waste depth squared is maximum. Conversely, the weakest waste is one in which the modulus divided by the depth squared is a minimum.

As discussed in Section 3.2, preliminary analyses were performed using three element types that represented different constituent stress laws. The hyperelastic element type was quickly found to be unstable when applied to the homogeneous waste models. Even with the stiffest material (150 in. and 120,000Pa shear modulus), the element predicted very large strains (thousands of percent) after the transient progressed to near the half-way point. The element type was abandoned in favor of the viscoelastic and isoparametric elements.

8.1 Homogeneous Solid Waste

The homogeneous solid waste model assumes that the material in the tank is an elastic-plastic medium with a 5% gas volume fraction. Two yield strengths, 300 Pa and 6,000 Pa, were evaluated in the model as were two waste heights: 150 in. (381 cm) and 300 in. (762 cm). The material properties that were assumed are shown in Table 8.1.1.

Table 8.1.1. Material Properties of Homogeneous Solid Waste

Shear Strength (Pa)	300	6,000
Elastic Yield Strain Limit	5%	5%
Shear Modulus (Pa)	6,000	120,000
Mean Depth Bulk Modulus (Pa) @ 150 in.	2,820,000	2,820,000
Mean Depth Bulk Modulus (Pa) @ 300 in.	3,550,000	3,550,000
Bulk Modulus Assigned (Pa)	3,550,000	3,550,000
Young's Modulus (Pa)	18,000	365,000
Tensile Strength (Pa)	900	18,000
Poisson's Ratio Calculated @ 150 in.	0.4989	0.4790
Poisson's Ratio Calculated @ 300 in.	0.4992	0.4833
Poisson's Ratio Used	0.499	0.483

All four parametric conditions were run using the viscoelastic and isoparametric element types. In the preliminary analyses, identical conditions were assumed for the material; the damping was assumed to be zero, and no strain hardening was assigned. The viscoelastic element models proved to be more unstable in executing the entire DBE transient. For the waste model of 150 in. height and a shear strength of 300 Pa, the material undergoes significant yielding (where more than 10% of the waste exceeds the elastic limit) about 7 seconds into the transient. The greatest strains are predicted to occur near the surface of the waste. At about 17 seconds into the transient, plastic strains are developed throughout the tank, but the maximum is still near the surface around the center of the tank. Just as the earthquake reaches the decay point (20 seconds into the transient), the peak plastic strain is 63% with possibly one-third of the tank exceeding 10% plastic strain. The deformation at this instant is illustrated in Figure 8.1.1.

With a depth of 300 in. (762 cm) and shear strength of 300 Pa, the stiffness is reduced so that the magnitude of plastic strain is much greater. The ANSYS analyses entered into a high-iteration equilibrium computation process where the time steps were progressively reduced and finally terminated before they reached the full 23-second seismic event period. Several methods were subsequently used to help stabilize the models, including plastic hardening and finite damping. These improved the solution process, but the peak plastic strain, although very localized, reached several hundred percent. Less than 15% of the tank reached 100% plastic strain, and all of that region is close to the surface. The final two weakly "stiff" slugs (300 in. waste depths) ran through about half the DBE transient before becoming nonconvergent. Therefore, while not accomplishing a final excited state of waste at the end of the postulated earthquake, they both showed results similar to the two 150-in. waste models. All exhibited very large plastic strains near the surface and significantly reduced strains in the interior of the tank.

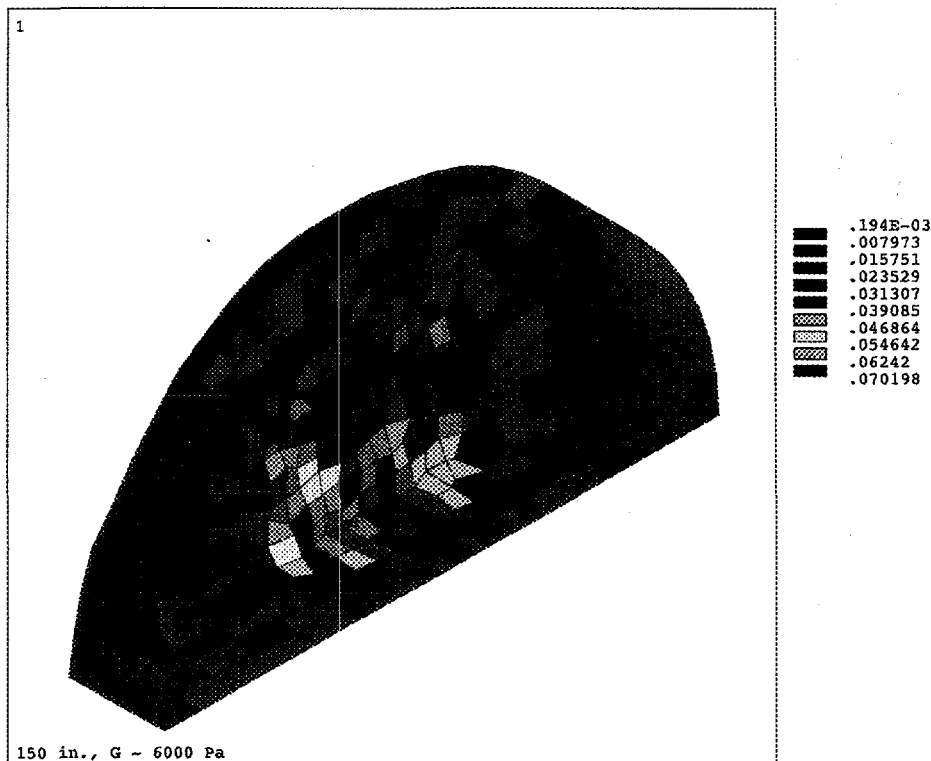


Figure 8.1.1. Viscoelastic Model Strain for 150 in., 300 Pa Shear Strength Waste

Analyses with the isoparametric element produced similar motion except that the variation in strain through the depth of the waste was less. The 300 in. (762 cm) and 300 Pa shear strength waste is the least stiff tank, 20 times weaker than the 6,000 Pa shear strength waste based on the beam stiffness analog (Eq. 8.1). The peak plastic strain in the waste reached 166% with most of the large strain near the top of the tank. The waste showed 18% peak plastic strain about 10 seconds into the event. The peak plastic strain was confined to the region near the waste surface and less than 0.5% of the tank had plastic strain that reached 100%. Indeed, more than half the tank and all of the waste in the lower half experienced less than 10% strain. This is shown graphically in Figure 8.1.2. The surface wave phenomenon can be observed in the deformed motion plot that accompanies the strain contours.

The homogeneous waste model with the highest stiffness is the 150 in. (381 cm) waste height model with a shear strength of 6 kPa. When subjected to the DBE, this material remained unyielded well into the transient. Plastic strain begins to occur near the middle of the tank at about 10 seconds. By the end of the seismic event, plastic strains are developed throughout the tank, but the peak plastic strain is still only 21%.

The 300 in. (762 cm), 6 kPa waste configuration exhibits similar strain history. The peak strain is about 18% and occurs at the end of the seismic event. No part of the tank volume has developed plastic strain in excess of 100% in either the 300- or 150-in.-deep tank. The strain contours for the 300-in.-deep, 6 kPa case is shown in Figure 8.1.3. Interestingly, the greatest strains occur near the free surface and not at the bottom as they would if the simple elastic beam analogy were assumed. The peak strain for both the 150- and 300-in. configurations with the 300 Pa shear strength waste occurred near the surface, at roughly 10–12% depth. Both the 6,000-Pa shear strength waste configurations exhibit peak strains deeper, at about half the waste depth.

Figure 8.1.4 shows the development of peak strains for the four homogeneous waste cases throughout the entire earthquake transient. Table 8.1.2 summarizes the global simulation results,

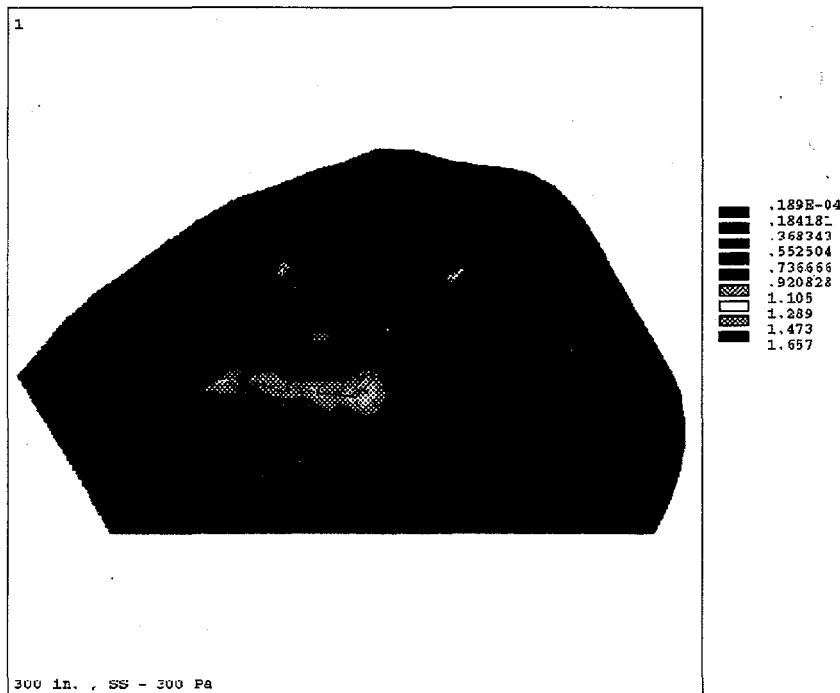


Figure 8.1.2. Peak Strain Contours for 300 in., 300 Pa Shear Strength Homogeneous Waste

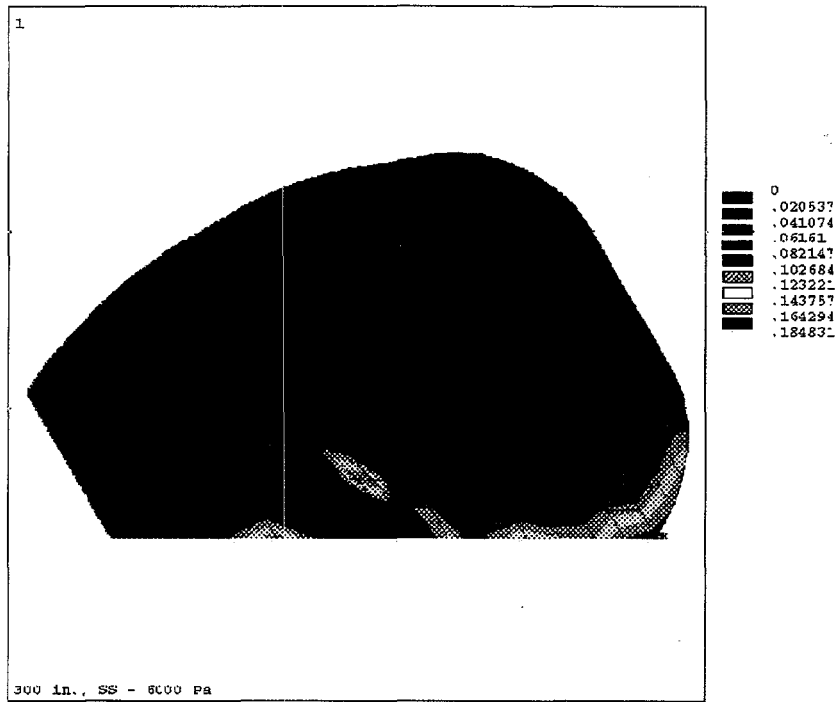


Figure 8.1.3. Peak Strain Contours for 300 in., 6,000 Pa Shear Strength Homogeneous Waste

showing both the maximum strain and the volume of waste exceeding 100% or greater plastic deformation. It is apparent that, for the three stiffest cases, none of the waste exceeds the shear strain limit (SL) criterion for gas release. Only the least stiff waste exhibits yielding, but only 5% of the volume exceeds 100% plastic strain.

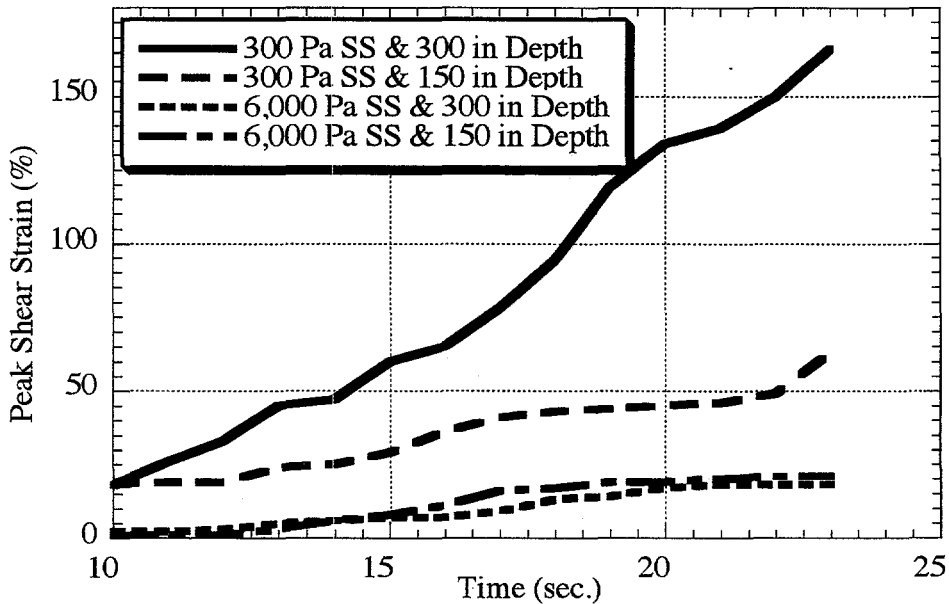


Figure 8.1.4. Time History of Homogeneous Waste Peak Shear Strain

Table 8.1.2. Summary of Results for Homogeneous Waste Configuration

Homogeneous Waste Configuration	Viscoelastic Material		Isoparametric Material	
	Peak Strain	Vol. >SL	Peak Strain	Vol. >SL
300 Pa Shear Strength - 150 in.	70%	~0%	63%	~0%
300 Pa Shear Strength - 300 in.	170% ^(a)	<10% ^(a)	166%	~0.5%
6,000 Pa Shear Strength - 150 in.			21%	~0%
6,000 Pa Shear Strength - 300 in.			18%	0%

(a) Estimate at about 17 seconds into the transient.

These results exhibit two important points. One is that little of the waste reaches 100% plastic strain for the stiffer configurations. The significance of this is that the strain limit criterion on potential gas mobilization assumes that material yields enough at 100% strain to allow retained gas to migrate. Only the weakest waste exhibits large plastic strain (shear strain >100%) in a limited volume late in the transient. The remaining waste models show virtually no plastic deformation that exceeds 100% as the material becomes more stiff.

The second important observation is that the plastic motion is far more severe near the surface than it is a meter or two below the surface. Therefore, most of the plastic strain, and therefore absorbed energy, develops near the surface of the tank. Deformed views of the waste indicate that there are surface waves developing at the upper free surface. These waves allow large plastic strain to occur locally because the surface is not restrained and the result will be to absorb large amounts of energy. Time sequence video of the waste shape action distinctly shows the rapid movement about the surface of these waves in addition to their increasing violence as the DBE transient progresses.

In addition to the plastic strain criterion, the shear strain energy density is also analyzed for these four cases. The time histories of peak energy density for the four tank waste configurations are shown in Figure 8.1.5. The weakest waste configuration (300 Pa shear strength and 300 in. waste depth) shows the largest peak shear strain energy density. Neither of the two 6,000 N-m/m³ shear strength waste tank configurations exceeds this gas mobilization criterion. Both of the 300 N-m/m³ shear strength waste cases exceeded the strain energy density criterion in a part of the volume.

Yielding and gas mobilization is assumed to occur at a shear strain energy density of 300 N-m/m³ (0.0428 in.-lb/in.³) for 300 Pa shear strength waste and at 6,000 N-m/m³ (0.856 in.-lb/in.³) for 6,000 Pa shear strength. The spatial distribution of strain energy density for the 300 in. deep, 300 Pa shear strength configuration is shown in Figure 8.1.6. Note that the units of strain energy density are in.-lb/in.³ for these contour plots. A peak strain energy density of 1000 N-m/m³ is equivalent to 0.1426 in.-lb/in.³ or psi in ES units. The regions of highest strain energy density compare with the regions of highest plastic strain (see Figure 8.1.2). A similar plot of strain energy distribution for 300 in. deep and 6,000 Pa shear strength tank waste is shown in Figure 8.1.7. Table 8.1.3 tabulates the percentage of the strain energy density limit (SEDL) and the fraction of the waste volume exceeding the SEDL for the four homogeneous waste cases.

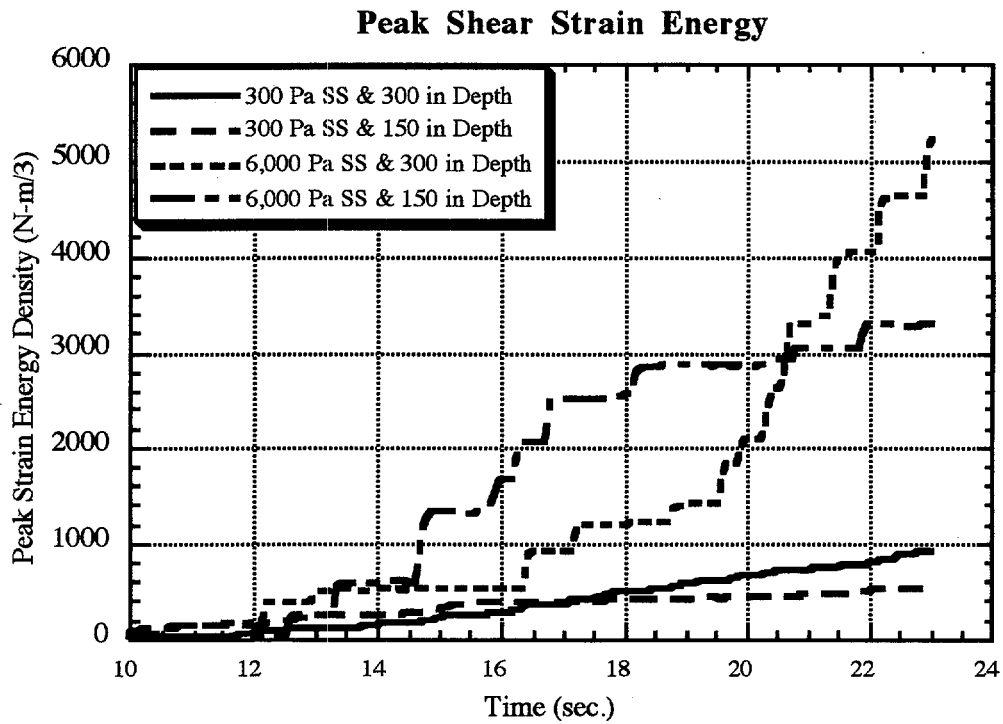


Figure 8.1.5. Time History of Peak Strain Energy Density (homogeneous waste)

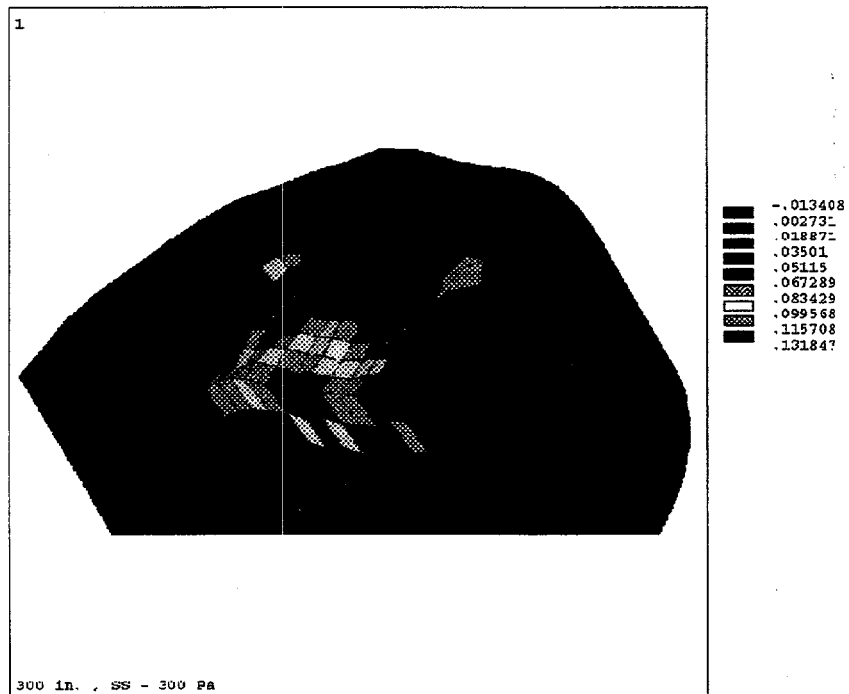


Figure 8.1.6. Strain Energy Density Distribution for 300 in., 300 Pa Shear Strength Waste

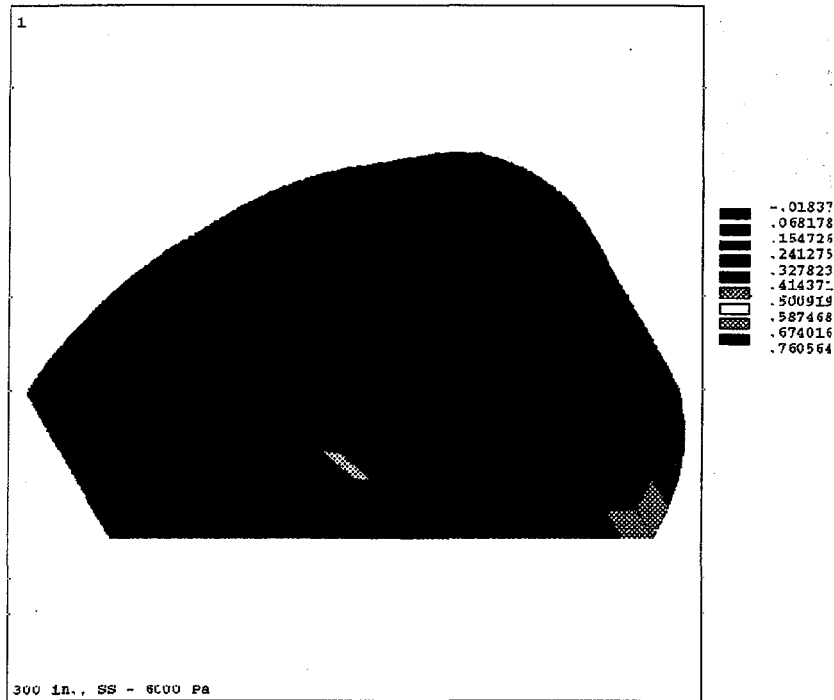


Figure 8.1.7. Strain Energy Density Distribution for 300 in., 6,000 Pa Shear Strength Waste

Table 8.1.3. Peak Plastic Strain Energy Density

Homogeneous Waste Configuration	Peak SED (% of Limit)	Volume > SEDL
300 Pa Shear Strength - 150 in.	188%	5.2 %
300 Pa Shear Strength - 300 in.	308%	12.8 %
6,000 Pa Shear Strength - 150 in.	57%	0 %
6,000 Pa Shear Strength - 300 in.	89%	0 %

The time history of volume of waste exceeding the SEDL gas mobilization criterion is shown in Figure 8.1.8 for the two homogeneous waste cases that exceeded the limit. The SEDL is 300 N-m/m^3 for the 300 Pa shear strength material and $6,000 \text{ N-m/m}^3$ for the 6,000 Pa strength material. For the weakest (300 Pa shear strength and 300 in. depth), the volume exceeding the 300 N-m/m^3 shear strain energy density reaches 12.8% at the end of the DBE event. This compares with only 0.5% of the waste based on the shear strain criterion. The predicted gas release potential is much larger based on the strain energy criterion than on the 100% strain criterion. Only 5% of the waste in the 300 Pa shear strength, 150 in. depth case exceeds the criterion. In comparison, no portion of the waste exceeded the shear strain limit criterion (100% strain). None of the waste in the two stiffest waste configurations (6,000 Pa shear strength) exceeded the strain energy criterion limit; the same was true of the shear strain limit criterion.

A cardinal assumption of the elastic plastic modeling is that the elastic shear stresses are small compared with the peak plastic stress obtained during the DBE. The basis for this assumption is laid out in Section 6. The plastic stresses are assumed to be shear because the material

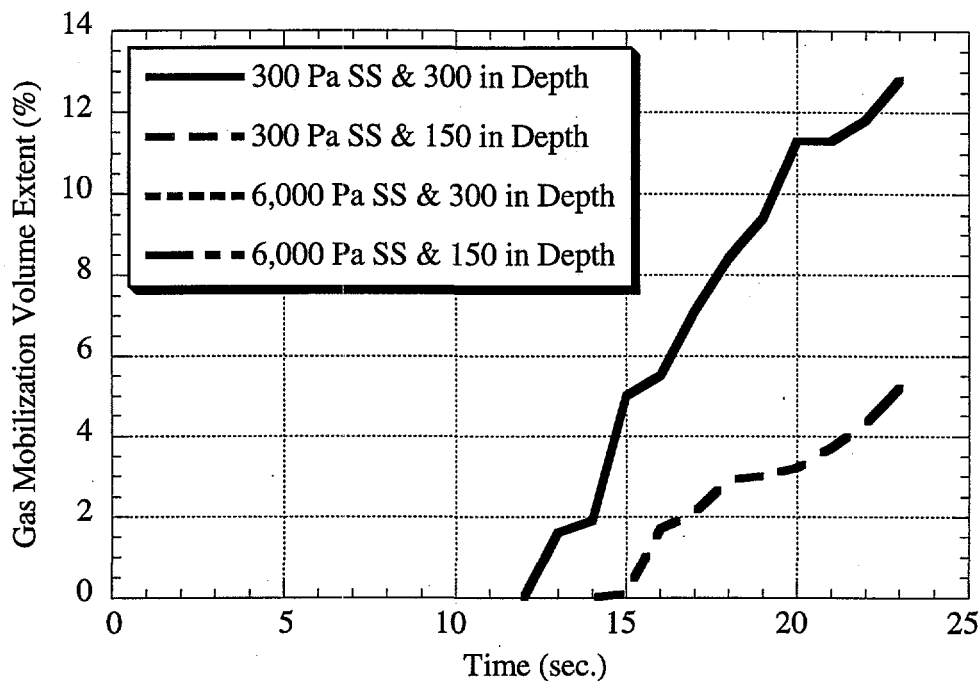


Figure 8.1.8. Time History of Waste Volume Exceeding Shear Strain Energy Density Limit

becomes totally incompressible when plastic, and no tensile stresses are produced. A comparison of plastic and elastic shear strain energy density for the 300 in. depth, 300 Pa shear strength solid can be observed in Figure 8.1.9. The total strain energy density is a sum of the elastic and plastic shear, so the elastic can be seen as a cyclic perturbation from the plastic energy curve.

During the DBE, cyclic dilatational pressure “waves” caused by elastic bulk compressive forces occur in all waste configurations. The origin of these stresses is discussed in Section 6. These pressures are greatest near the floor of the tank, where the amplitude of the applied shock conditions is passed directly to the waste. In contrast, the location of maximum shear stress and strain is near the waste surface. A comparison of the shear and hydrostatic stresses for the maximum shear strain location for the 300 in. deep, 300 Pa shear strength case is shown in Figure 8.1.10. The cyclic hydrostatic pressure waves “ring” through the tank at about 2 Hz. The hydrostatic pressure oscillations vary with a magnitude of about 22,000 Pa (3 psi) around the local gravitational gauge pressure, which is about 13,000 Pa (1.8 psi) for this case (following structural mechanics convention, the hydrostatic pressure is negative because it is compressive).

The differentiation between hydrostatic dilatation and plastic strain can also be seen in the strain energy density. Figure 8.1.11 compares the total strain and plastic strain energy densities for the same location in the 300 in., 300 Pa shear strength case. The strain energy densities are always positive since the definition involves a signed stress multiplied by its companion strain. When stresses are compressive (negative), the corresponding strains are also negative. Peak elastic hydrostatic strain energy densities are two orders of magnitude greater than the shear strain energy density limit.

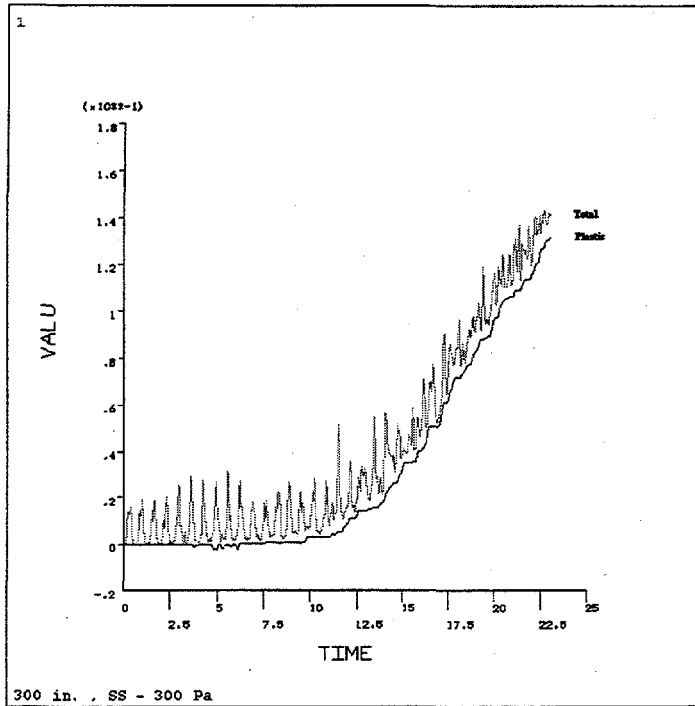


Figure 8.1.9. Time History of Peak Plastic and Total (elastic and plastic) Strain Energy Density

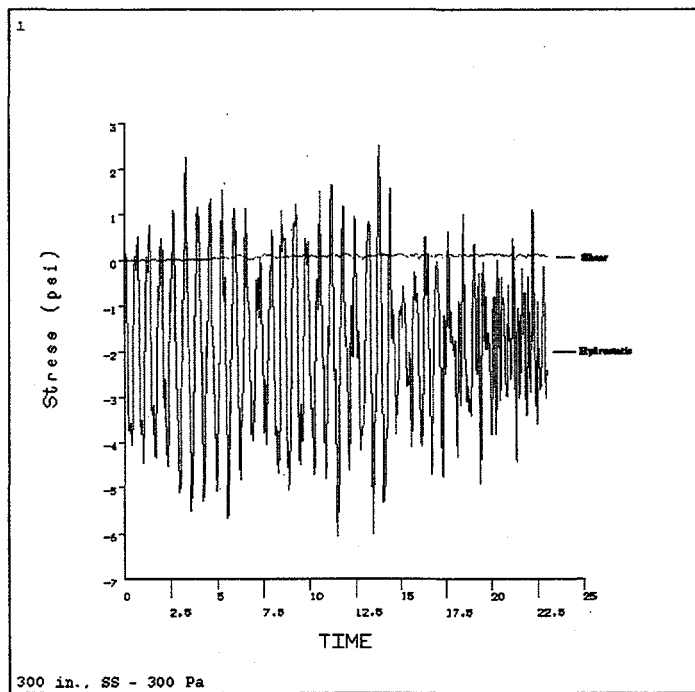


Figure 8.1.10. Time History of Peak Plastic Shear and Hydrostatic Stresses

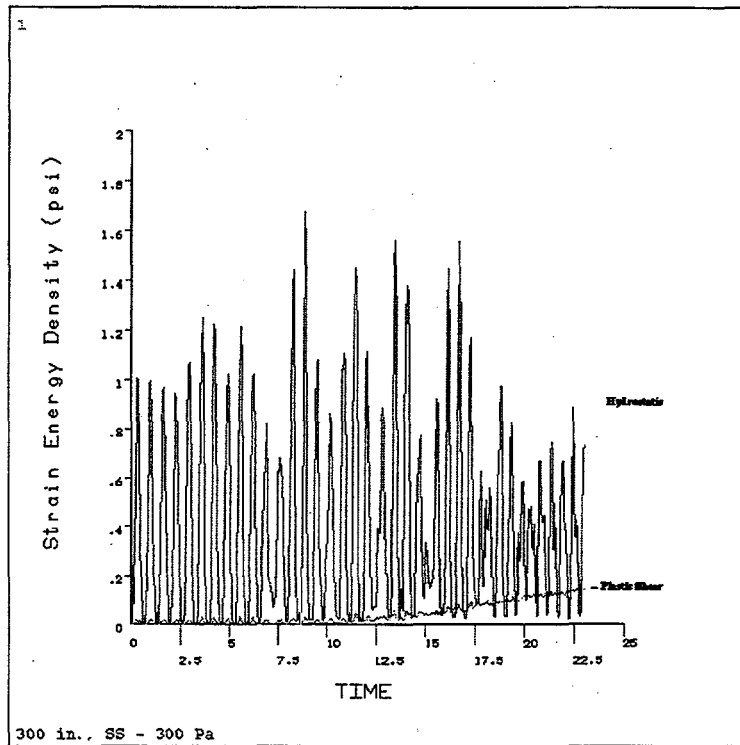


Figure 8.1.11. Time History of Peak Plastic and Hydrostatic Strain Energy Densities

The hydrostatic stresses vary with depth with the cyclic variation greatest near the bottom. Figure 8.1.12 shows the hydrostatic pressure fluctuations at three depths for the 300-Pa shear strength, 300-in. depth case. At the location of peak plastic strain near the surface in each waste configuration, the envelope of hydrostatic pressure variations is about 22,000 Pa (3 psi) for the 300 Pa shear strength waste and about 112,000 Pa (16 psi) for the 6,000 Pa shear strength waste. The amplitudes increase with depth such that the envelopes near the bottom of the tank are about 105,000 Pa (15 psi) and 280,000 Pa (23 psi) for the 300 and 6,000 Pa shear strengths, respectively. Since the nominal hydrostatic pressure increases with depth, as does the amplitude of the fluctuation, the minimum gauge pressure (the difference between wave amplitude and local mean gravitation hydrostatic pressure) is a rather constant vacuum of about 35,000 to 56,000 Pa (5 to 8 psi) maximum below ambient.

As outlined in Section 6, it is difficult to prescribe a failure criterion corresponding to these hydrostatic pressure waves based on contemporary knowledge of waste yielding. The present argument derived from barometric pressure response investigations proposes that the dilatational strains primarily are absorbed in the expansion and contraction of bubbles. If we assume that the gas bubble volume change obeys the ideal gas laws, then the dilatational strain of the bubble correlates directly with the hydrostatic pressure wave. Near the waste surface, the average volume change of a bubble would be about 20% for the 300 Pa shear strength waste and about 30% for the 6,000 Pa strength, ignoring inertial damping effects. This corresponds to a change in diameter of 6 to 10%. At the bottom of a 300 in. tank, the average volume change would range from 45 to 60% for 300 and 6,000 Pa shear strength waste, respectively, with a corresponding diametral fluctuation of 15 to 20%.

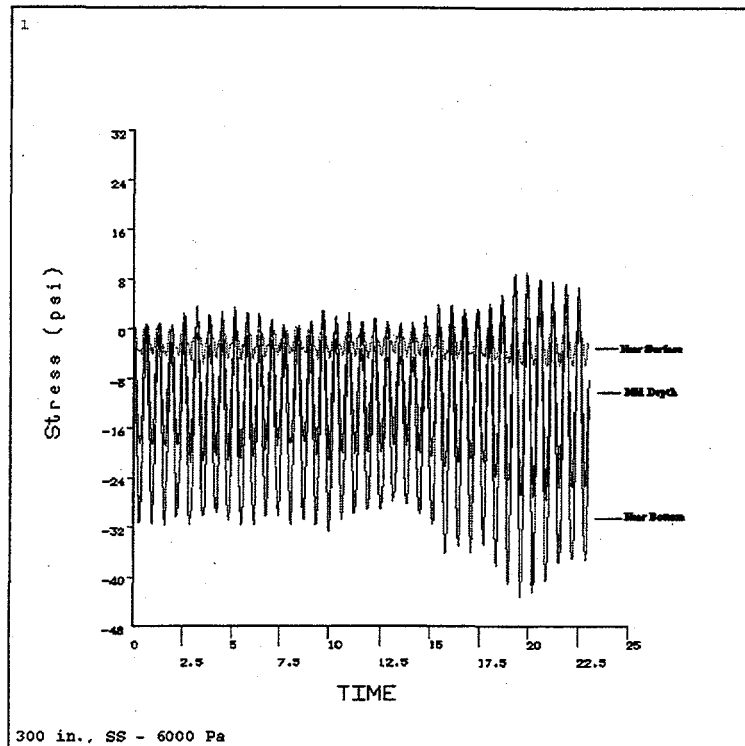


Figure 8.1.12. Time History of Hydrostatic Stresses at Three Waste Depths

8.2 Liquid-over-Solid Waste

All of the analyses performed for the liquid-over-solid waste configuration used ANSYS isoparametric elements. The material model for the solid was identical to that used for homogeneous waste with the same elastic-plastic yielding assumptions. The liquid was assumed to be an incompressible elastic material that exhibited no shear or tensile strength stress or strains except hydrostatic.

The liquid-over-solid waste model assumes that the waste is made up of an elastic-plastic solid media over the lower half covered by an incompressible, hydrodynamic fluid over the top half. The solid portion of the waste is assumed to have a 5% gas volume fraction. The solid waste has a yield strength and undergoes strain-induced stress, while the liquid exhibits hydrostatic stresses only. Two yield strengths, 300 and 6,000 Pa, were considered for the solid, with two overall waste heights of 300 (762 cm) and 400 in. (1,016 cm) to make four parametric cases for this configuration. The liquid and solid depths were assumed to be equal, so a waste height of 300 in. had 150 in. of solids and 150 in. of liquid. The material properties assigned for the solids are shown in Table 8.2.1. The bulk modulus and Poisson's ratio are based on the midpoint depth of the solids layer. For consistency with the analysis approach discussed in Section 5, the moduli for all depths is assumed to be the same as that for the assigned homogeneous waste.

Table 8.2.1. Material Properties of the Solid in the Liquid-over-Solid Waste

Shear Strength (Pa)	300	6,000
Elastic Yield Strain Limit	5%	5%
Shear Modulus (Pa)	6,000	120,000
Mean Depth Bulk Modulus (Pa) @ 300 in.	3,622,600	3,622,600
Mean Depth Bulk Modulus (Pa) @ 400 in.	4,107,400	4,107,400
Bulk Modulus Assigned (Pa)	3,550,800	3,550,800
Young's Modulus (Pa)	18,013	365,185
Tensile Strength(Pa)	900	18,013
Poisson's Ratio Calculated @ 300 in.	0.4991	0.4836
Poisson's Ratio Calculated @ 400 in.	0.4993	0.4855
Poisson's Ratio Used	.499	.483

The predicted response of the solid waste that is covered by liquid is somewhat more violent than the homogeneous waste. The liquid simply acts as an elastic coupler generating hydrostatic pressures to the surface of the solid waste below. Since it acquires no stresses other than hydrostatic and is assumed to contain no gas, it is deleted from the processed graphic results from the ANSYS analyses (Figures 8.2.1 through 8.2.6). The predicted peak strains in the solids are larger than in the homogeneous waste. Figure 8.2.1 presents the peak strain time history for the four parametric cases in this waste configuration. For 300 Pa shear strength cases, the peak strains are 1600 and 750% for the 400 and 300 in. depth, respectively. The 6000 Pa shear strength cases exhibit only 27 and 8% peak strain for the 400 and 300 in. deep waste, respectively.

The solid's response exhibits the large surface wave motion similar to the behavior of the homogeneous waste models. Peak plastic strains exceed 100% beginning about 8 seconds into the DBE for the 400 in. depth waste and 10 seconds for the 300 in. depth waste with 300 Pa shear strength. There is an almost linear increase in peak strain with time for both of these waste depth configurations. The 400 in. depth, 6,000 Pa shear strength, the configuration shows no plastic strain until 10 seconds into the seismic event and has a peak strain similar to the 300 in. depth homogeneous waste. For the last parametric case, 300 in. depth and 6,000 Pa shear strength, no plastic strain occurs before 10 seconds, and peak strains are less than the equivalent homogeneous case (8% compared with 23% in the homogeneous case).

The large surface waves are apparent in the plastic strain contour plot shown in Figure 8.2.2 for the weakest waste configuration, 300 Pa shear strength and 400 in. waste depth. The liquid layer is not shown on the plastic strain contour plots to allow visualization of the solid strain distribution. The most severe plastic strain can be seen at the tank center along the upper surface of the solid (the interface between the solid and liquid). This is consistent with the resonance of a liquid excited in a cylindrical tank. Concentric waves tend to occur, causing large axial deflections at the center of the tank. In the present model, liquid "floats" on a weak solid material so that the axial deflections can occur on the top and bottom surfaces. The liquid tends to act as an oscillator to amplify the motion of the solid surface. This results in much larger peak strains than in the homogeneous case for the same shear strength.

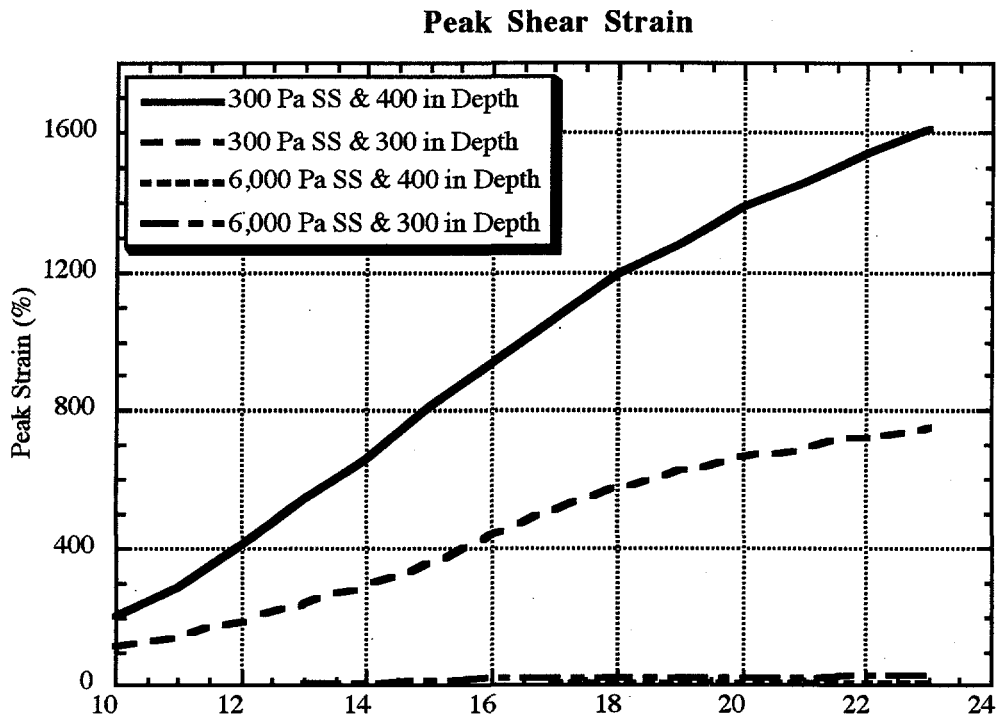


Figure 8.2.1. Time History of Liquid-over-Solid Waste Tank Peak Shear Strain

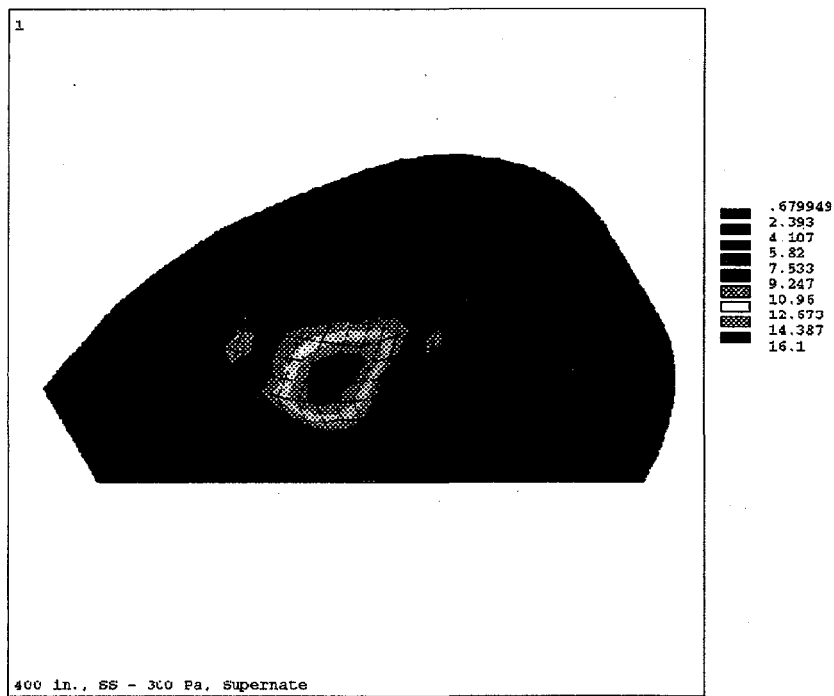


Figure 8.2.2. Peak Strain for 400 in., 300 Pa Shear Strength Waste (liquid over solid)

This does not appear to be true for the stiffer waste, at least not during the 23-second DBE transient. The spatial variation in plastic strains for the 6,000 Pa shear strength waste with a 400 in. depth is shown in Figure 8.2.3. It exhibits some of the trends of the homogeneous waste results in that the peak strains are in the 20% range and near the center, below the surface. The lack of apparent coupling between the liquid and solid, as appeared in the 300 Pa shear strength solid, carries over to the 300 in. waste depth.

One obvious explanation is that the degree of material distortion versus dilatation (compressibility) is some 20 times smaller for the 300 Pa shear strength waste. This very weak material tends toward "liquidity" quicker and therefore couples better to the liquid layer where the stiffer solid material exhibits greater deviatoric resistance; thus, elastic shear and tensile strain resist liquefaction during a DBE. Since the ultimate transition into plastic makes the waste purely incompressible, it is the volume yielded, as well as the stiffness, that ultimately sets up this coupling.

The volume of plastic strained waste grows with time, as it did with the homogeneous waste. As might be expected from the much larger peak plastic strains, the extent of potential gas mobilization is much greater. As shown in Figure 8.2.4, the 300 and 400 in. depth, 300 Pa shear strength cases develop sizable mobilized volumes based on the 100% strain criterion. Note that the fraction of the volume mobilized is based only on the solid's volume, which is one-half the total. A total of 85% of the solid volume exceeds the strain limit in the 400 in. deep waste, while 37% does so in the 300 in. case. Both of these cases exhibit a declining rate of potential gas mobilization toward the end of the DBE transient. Neither of the 6,000 Pa shear strength cases had any waste exceeding the 100% strain criterion. Predicted peak strain and the peak volume mobilized are compared in Table 8.2.2.

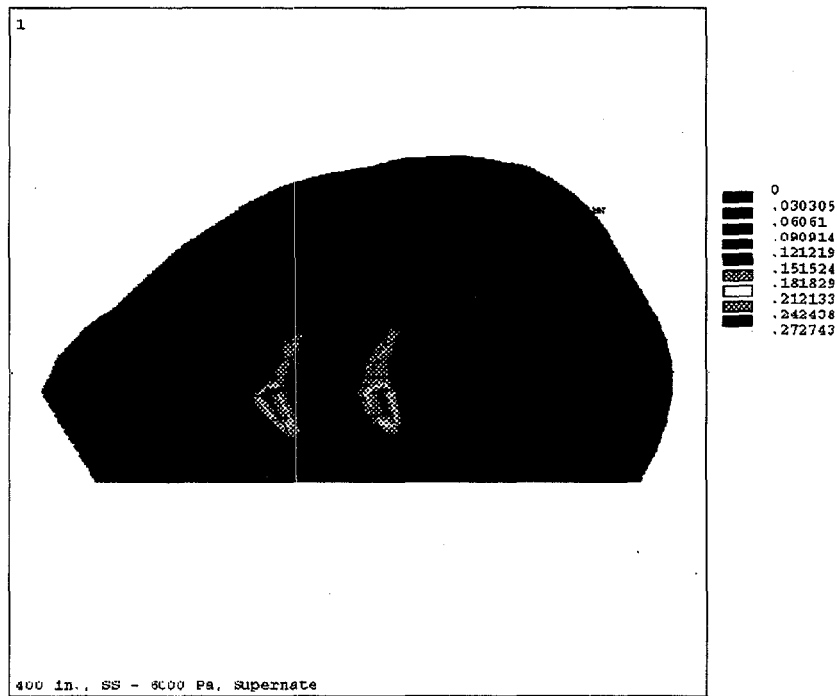


Figure 8.2.3. Peak Strain for 400 in., 6,000 Pa Shear Strength Waste (liquid over solid)

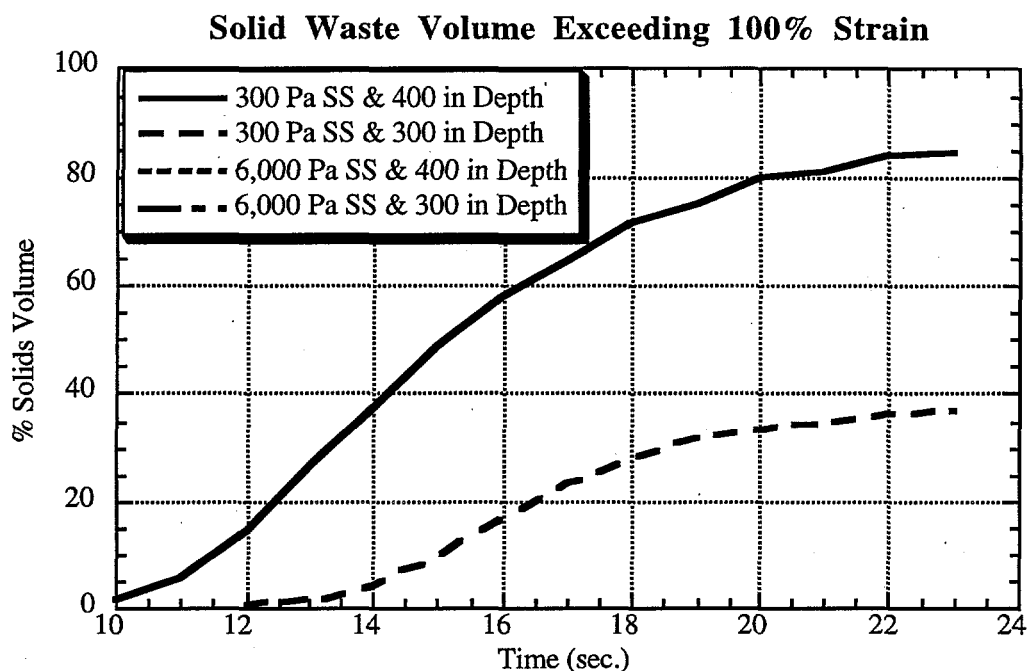


Figure 8.2.4. Time History of Volume Exceeding Strain Limit (liquid over solid)

Table 8.2.2. Peak Strain and Volume Exceeding Strain Limit Criterion

Liquid-over Solid Configuration	Peak strain (%)	Vol.>SL (% of Solid)
300 Pa Shear Strength - 400 in.	1610	85%
300 Pa Shear Strength - 300 in.	749	37%
6,000 Pa Shear Strength - 400 in.	8	0%
6,000 Pa Shear Strength - 300 in.	27	0%

The predicted strain energy density is also larger for the liquid-over-solid waste configurations than for the homogeneous waste. This follows the larger plastic (shear) strains that are developed during the DBE. For the 400 in. deep waste configuration, the distribution of plastic strain energy density is presented in Figure 8.2.5 for 300 Pa shear strength and in Figure 8.2.6 for the 6,000 Pa shear strength cases. Again, the liquid cover is not shown to allow visualization of the solid strain energy density distribution. These plots are shown in ES units of in.-lb/in.³.

Here, too, the elastic shear is assumed to be small compared with the plastic (shear) strain. A comparison of plastic and elastic shear strain energy density at the location of peak total strain energy density for the 400 in. deep, 300 Pa shear strength solid can be observed in Figure 8.2.7. The total strain energy density is a sum of the elastic and plastic shear, so the elastic strain energy density can be seen as a cyclic perturbation from the plastic energy curve. The peak variation in elastic shear strain energy density is about ± 0.12 in.-lb/in.³ (827 N-m/m³) compared with the peak plastic strain energy density for that location of 1.8 in.-lb/in.³ (12,410 N-m/m³).

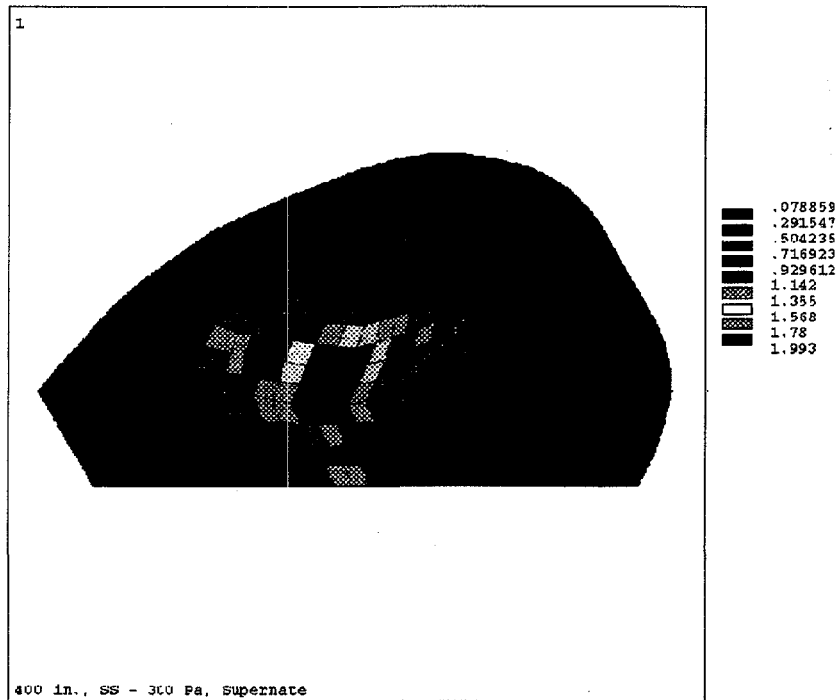


Figure 8.2.5. Strain Energy Density for 400 in., 300 Pa Shear Strength Waste (liquid over solid)

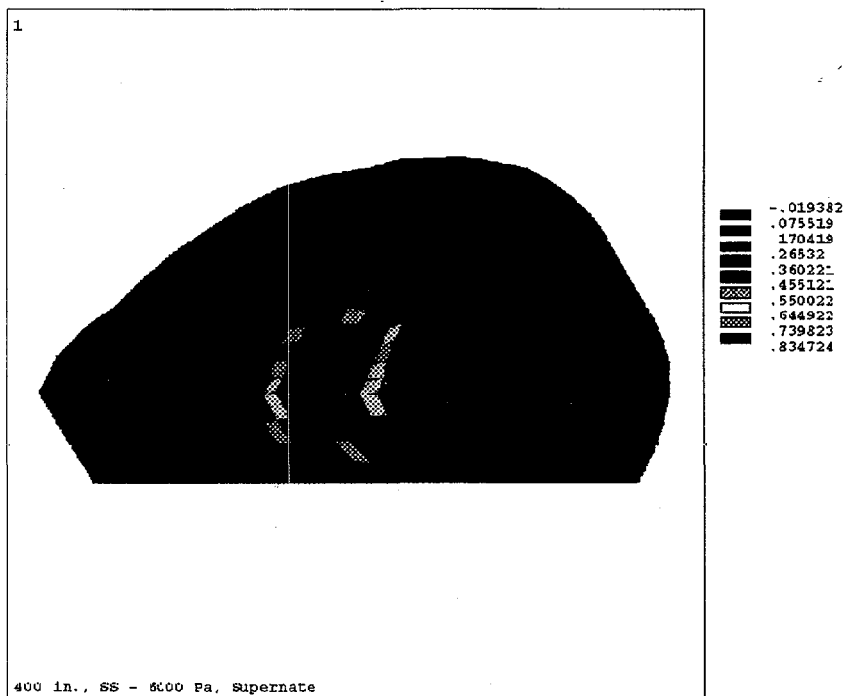


Figure 8.2.6. Strain Energy Density for 400 in., 6,000 Pa Shear Strength Waste (liquid over solid)

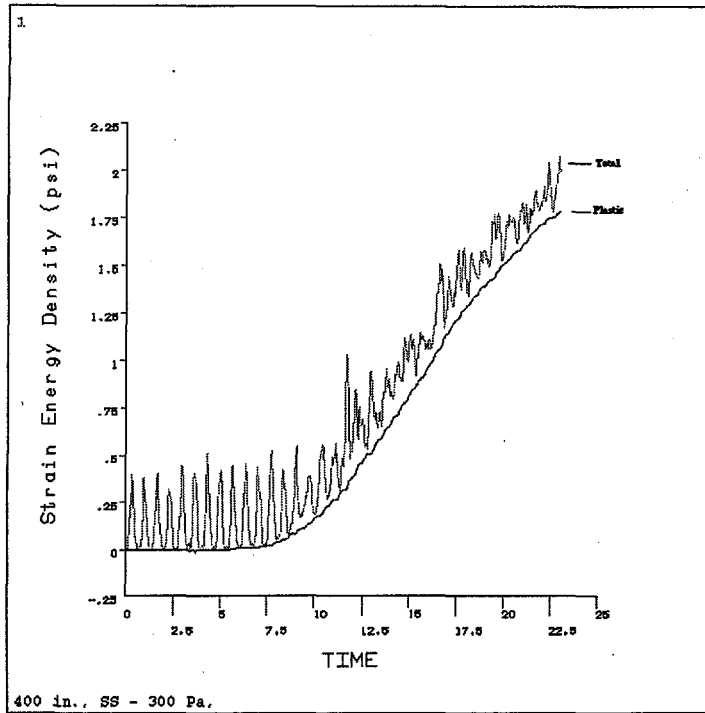


Figure 8.2.7. Time History of Peak Plastic and Total (Elastic & Plastic) Strain Energy Density (Liquid-over-Solid)

These cases also exhibit periodic elastic shear motion similar to the homogeneous tank models. The frequency is about 1 Hz for the 400 in. deep tanks and roughly 2 Hz for the 300 in. deep tanks. This variation follows the simple beam elastic model, where frequency varies with the square of the length of the vibrating component, in this case, depth. The actual driver of the harmonic is hydrostatic waves similar to those observed in the homogeneous waste models. It shows up in the elastic shear motion because shear can be tied to the orthogonal components of the volumetric strain.

Figure 8.2.8 shows the periodic variation of total strain energy density with depth for the weakest waste (400 in. deep and 300 Pa shear strength). A comparison of total (elastic and plastic) shear strain energy density for two different depths is presented. One curve represents the location of the peak strain and the other the location of the peak strain energy density. The peak oscillation about the rising mean varies from about 1.8 in.-lb/in.³ (12,410 N-m/m³) at the surface to about 0.4 in.-lb/in.³ (2,750 N-m/m³) near the bottom of the tank. The distribution through the waste height is approximately linear, so the middle of the solid waste is an average of the upper surface and floor energy densities. The strain energy densities rise quickly from a point 10 seconds into the DBE and decline slightly beyond about 17 seconds into the transient.

The time history of the peak strain energy density for the four parametric cases is shown in Figure 8.2.9. The strain energy densities are presented only for the solids. As with the homogeneous waste, the 6,000 Pa shear strength solids exhibit larger strain energies than the weaker, 300 Pa shear strength waste. The peak strain energy density for the 300 Pa shear strength solid with a 400 in. waste depth reaches 13,742 N-m/m³ compared with only 908 N-m/m³ for the 300 in. deep homogeneous waste. In fact, the peak strain energy density for the liquid-over-solid waste configuration is already twice the absolute maximum of the homogeneous waste 10 seconds

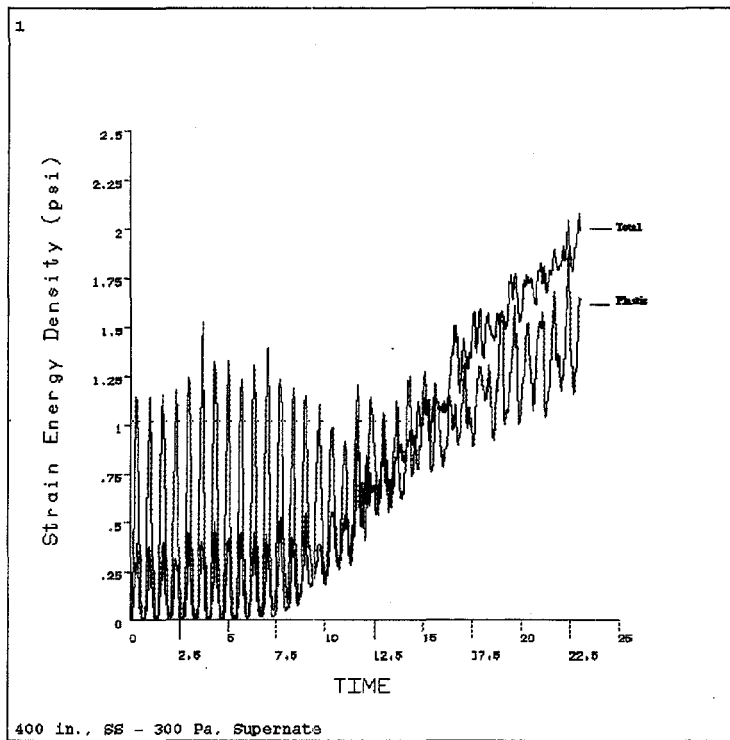


Figure 8.2.8. Time History of Peak Total (elastic and plastic) Strain Energy Density (liquid over solid)

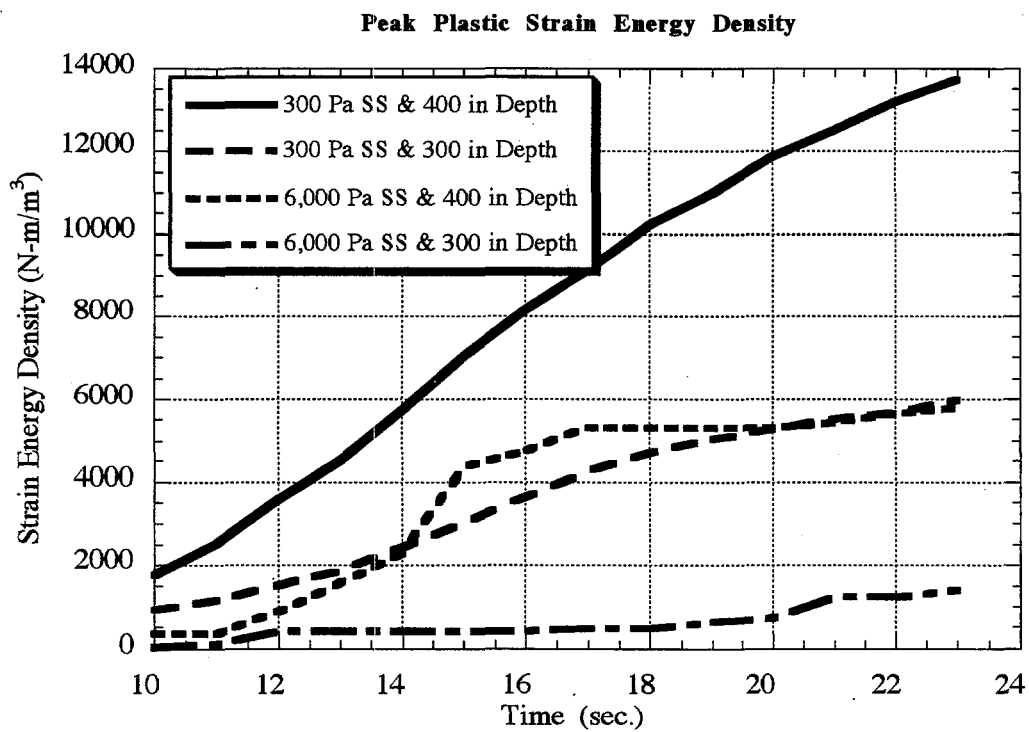


Figure 8.2.9. Time History of Peak Strain Energy Density (liquid over solid)

into the DBE transient and 15 times greater by the end. The stiff 6,000 Pa shear strength solids, on the other hand, show peak strain energy density trends similar to the homogeneous waste. The peak energy density for the 400 in. deep, liquid-over-solid configuration is 5,755 N-m/m³ compared with 5,245 N-m/m³ for the 300 in. deep homogeneous waste.

A time history of peak strain energy densities for four depths in the 400 in., 300 Pa shear strength waste is shown in Figure 8.2.10. The overall peak trend (the top line) is located on the surface of the waste, as indicated in Figure 8.2.5. The lowest trend line is near the floor of the tank. The time history lines that virtually overlay one another are for median depth locations in the waste; one is at the centerline of the tank and the other is at roughly the mid-tank radius position on a line 90° from the symmetry plane.

The weaker solids have a smaller strain energy density limit than the stiffer solid waste. The limit is 300 N-m/m³ (0.0428 in.-lb/in.³) for 300 Pa shear strength waste, and 6,000 N-m/m³ (0.856 in.-lb/in.³) for 6,000 Pa strength waste. As with the homogeneous waste, the 6,000 Pa shear strength solids in the liquid-over-solid waste exhibit no gas mobilization. The 300 Pa shear strength solids exceed the energy limit within several seconds of the DBE event.

Table 8.2.3 summarizes the peak plastic strain energy density as the percentage of the SEDL and the fraction of the solids volume exceeding the SEDL for each liquid-over-solid case.

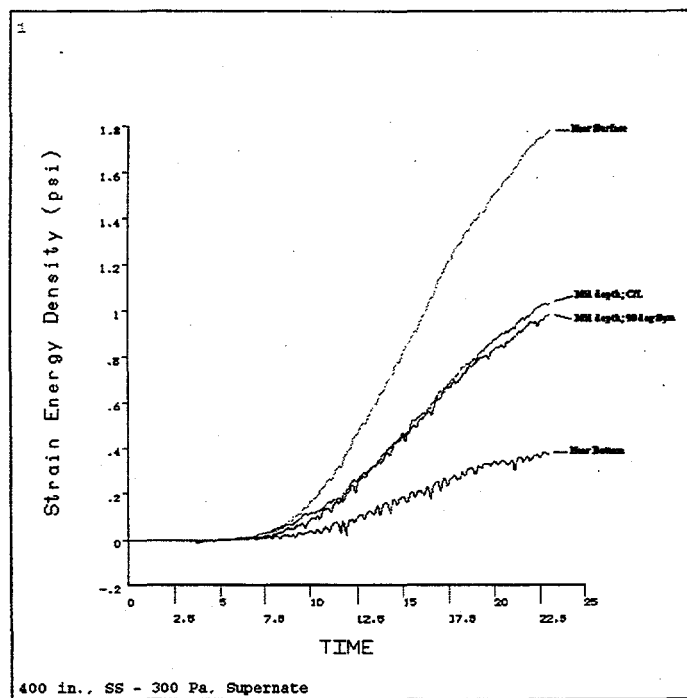


Figure 8.2.10. Time History of Peak Strain Energy Density with Depth (liquid over solid)

Table 8.2.3. Maximum Plastic Strain Energy Density

Tank Waste Parametric	Peak SED (% of limit)	Volume > SEDL (% of solids)
300 Pa Shear Strength - 150 in.	4580	98
300 Pa Shear Strength - 300 in.	1407	80
6,000 Pa Shear Strength - 150 in.	96	0
6,000 Pa Shear Strength - 300 in.	23	0

The time history of volume of solid waste exceeding the potential gas mobilization criterion is shown in Figure 8.2.11. None of the 6,000 Pa shear strength cases exceeded the energy limit in either waste depth. For the weaker, 300 Pa shear strength solid, the predicted gas mobilization in the 400 in. deep tank spreads throughout the waste quickly such that the volume climbs from a quarter of the solid at 10 seconds to all of it by 16 seconds. The 300 in. deep waste, which is slightly more stiff, follows closely, so that by the end of the DBE event 98% of the solid volume exceeds the energy limit criterion for gas mobilization.

It is apparent that gas mobilization for the liquid-over-solid waste configuration is rapid and complete based on the strain energy density limit criterion for weak (300 Pa shear strength) solid. The liquid layer induces larger strains and therefore strain energy densities in the solid than in the homogeneous waste for equivalent heights. The liquid, a basically an incompressible elastic medium, acts as a harmonic oscillator and develops sloshing modes that effectively push and pull on the solid layer, amplifying that layer's response. Stiff solids (6,000 Pa shear strength) would be unaffected by the DBE.

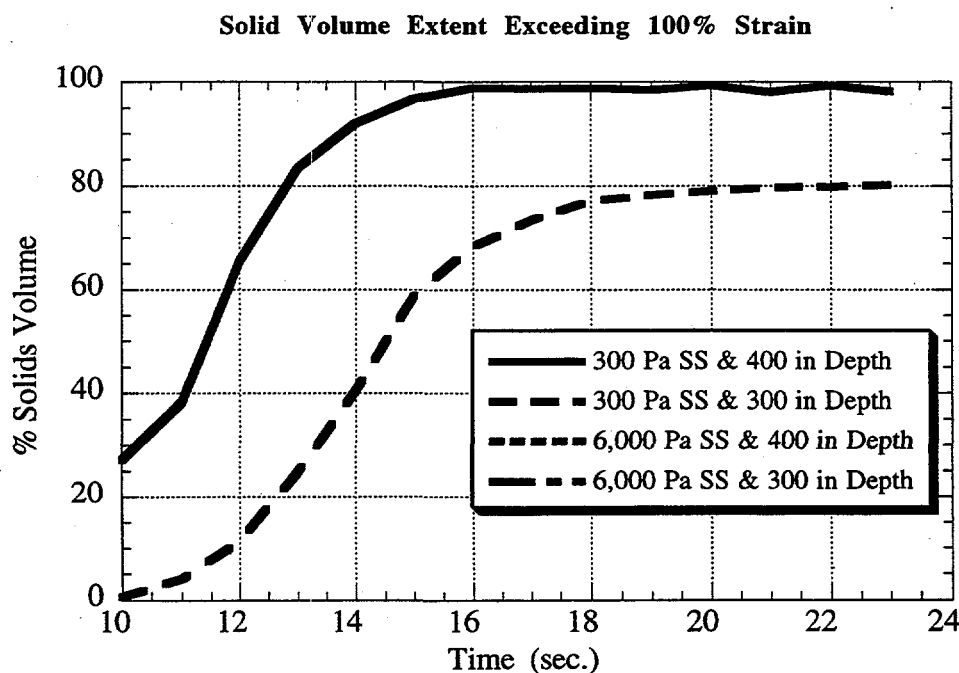


Figure 8.2.11. Time History of Volume Exceeding Strain Energy Density Limit (liquid over solid)

A comparison of the hydrostatic stress variation with depth is shown in Figure 8.2.12. The trend is similar to the results for the homogeneous waste. The pressure waves pass through the tank at a frequency of roughly 2 Hz. The absolute magnitude of the hydrostatic pressure pulses reaches some 56,000 Pa (8 psi) near the solid surface and 168,000 Pa (24 psi) near the floor. These pulses oscillate about the mean hydrostatic pressure due to depth, so that the median pressure increases (negatively on Figure 8.2.12) with depth. This results in an average minimum pulse pressure that is nearly atmospheric.

This study did not address the effects of different liquid-to-solid depth ratios. It is physically intuitive to assume that a smaller liquid depth decreases the violence of the coupled system response because liquid sloshing modes and displacements are driven inversely by the depth of the liquid. Wave frequencies increase but deflections decrease with decreasing liquid depth.

8.3 Solid-over-Liquid Waste

The analyses of solid-over-liquid waste simulates Hanford Tank 241-A-101 and use the ANSYS isoparametric element. The material model for the solid was identical to that used on the homogeneous waste with the same elastic-plastic yielding assumptions. For the liquid, an incompressible elastic material was initially used as it was in the liquid-over-solid models. The results for this element in the liquid-over-solid models indicated that it acts as a harmonic oscillator and exacerbates motion in the solid waste even when the liquid is on top of the solid. Waste configuration models that have this oscillator between the excitation (tank walls and floor) and the elastic-plastic solid (above the liquid) proved too unstable to perform full DBE transient response. It was not possible to obtain converged solutions after several seconds into the transient.

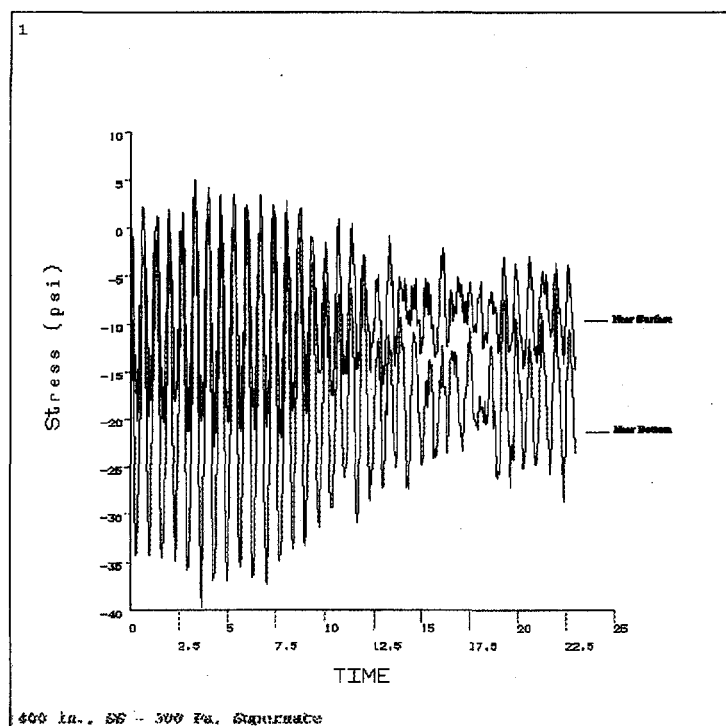


Figure 8.2.12. Time History of Hydrostatic Stresses at Two Tank Waste Depths (liquid over solid)

For this reason, the "liquid" model was switched to an isoparametric element with a Poisson's ratio that gives the bulk modulus of water. The solid-over-liquid model assumes that the waste is made up of an elastic-plastic solid covering an semi-incompressible weak elastic material. The solid portion of the waste is assumed to have a 14% gas volume fraction and is assigned a yield strength of 300 Pa. The material properties that are assigned for the solid are shown in Table 8.3.1.

The predicted response of the solid is somewhat similar to the liquid-over-solid models. The liquid simply acts as an elastic coupler generating hydrostatic pressures to the surface of the solid waste above. However, the predicted peak strains produced in the solid wastes are smaller than those experienced in the liquid-over-solid waste models. Figure 8.3.1 presents the time history of peak strain for this waste configuration. Only the strains in the solid are shown.

The most probable reason for the milder peak strains is the use of a semi-incompressible elastic solid instead of the hydrostatic fluid material type for the liquid. The liquid model exhibits some strain-induced shear stress, which dampens the response of the liquid. Since the liquid acts as an oscillator coupled to the solid, the solid exhibits less excitation during the seismic motion.

Because the liquid motion is more restrained than that of an elastic fluid material model, the predicted peak strains in the solid are probably not conservative. Based on results from liquid-over-solid models and from preliminary fluid material modeling of the liquid in this waste configuration, we would expect to see peak strains significantly greater than those being predicted. It is likely that the solid response would be similar to that resulting from the liquid-over-solid models.

The peak strain distribution for this tank configuration is shown in Figure 8.3.2. Unlike the other homogeneous and liquid-over-solid tank models, there are several regions of high localized strain. The strain levels generally lie below those of the liquid-over-solid models (see Figure 8.2.4). The lowest strain predicted at the end of the DBE for the liquid-over-solid tank is about 47% but an order of magnitude less for the solid-over-liquid model.

The probably nonconservative predictions of peak strain due to use of the solid material model for the liquid probably affects the estimates of gas mobilization based on the strain limit criterion. As with other waste models there are large surface waves, as suggested in Figure 8.3.2. The liquid layer is not shown in the plastic strain contour plots to allow visualization of the solid strains. The most severe plastic strain occurs roughly concentrically along the upper waste surface. There are also several regions near the center bottom of the solid layer (at the interface between the solid and the liquid).

Table 8.3.1. Material Properties of Solid-over-Liquid Waste

Elastic Yield Strain Limit	5%
Shear Modulus (Pa)	300
Mean Depth Bulk Modulus for a solid (Pa)	1,140,000
Mean Depth Bulk Modulus for a liquid (Pa)	1.2E+12
Young's Modulus (Pa)	18,013
Tensile Strength (Pa)	900
Poisson's Ratio for a solid	0.4974
Poisson's Ratio for a liquid	0.4999

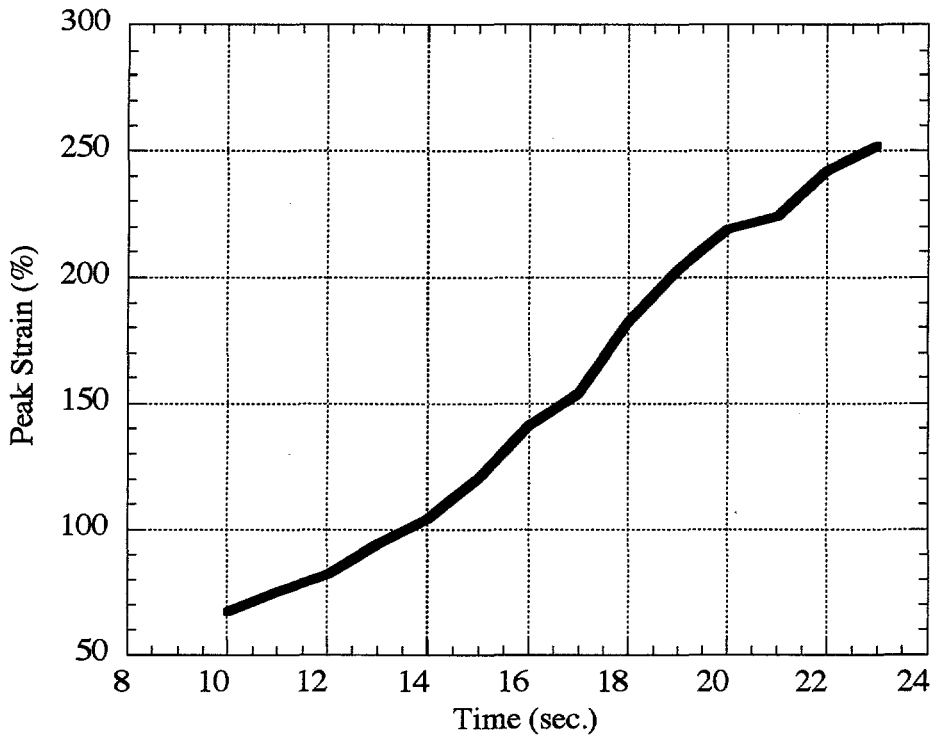


Figure 8.3.1. Time History of Peak Shear Strain (solid over liquid)

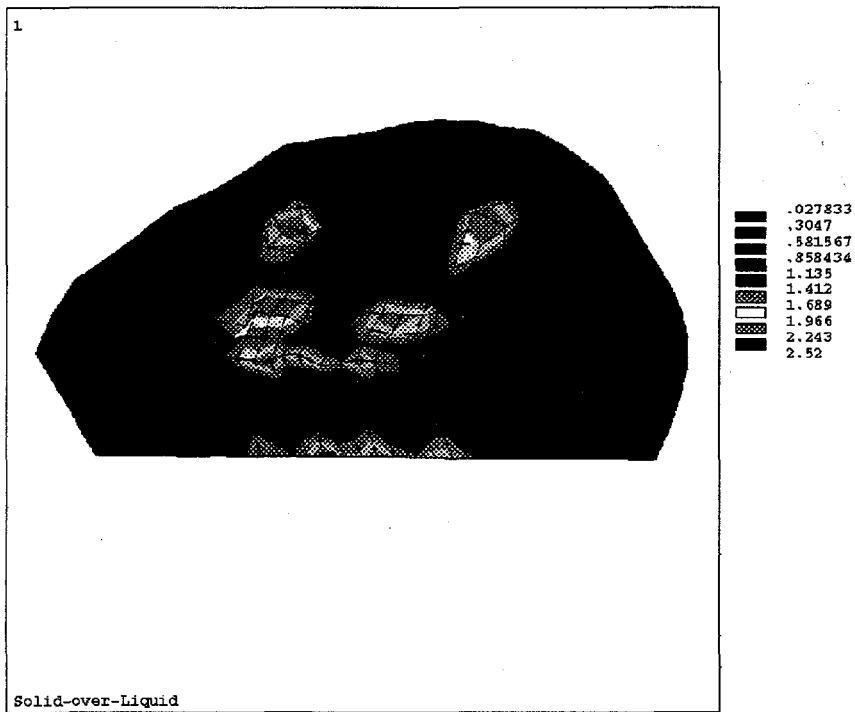


Figure 8.3.2. Peak Strain (solid over liquid)

The peak strain energy density is also less for the solid-over-liquid waste configurations than for the liquid-over-solid waste. This again follows the smaller plastic (shear) strains. The peak strain energy density is $2083 \text{ N}\cdot\text{m}/\text{m}^3$. Figure 8.3.3 shows the predicted peak strain energy density distribution at the end of the DBE. It is apparent that the peak strain energy densities generally occur at peak strain locations. It is not feasible to estimate the degree of nonconservatism in the strain energy density. The time history of the predicted strain energy density is shown in Figure 8.3.4.

The predicted gas mobilization based on the volume of waste exceeding the strain limit is roughly one-third of the liquid-over-solid model for 300 in. depth and 300 Pa shear strength. Figure 8.3.5 presents the time history of the fraction of solid volume mobilized. A peak extent of 12.6% is reached at the end of the DBE. The predicted volume based on the SEDL is also shown in this figure. The trend is similar to the results for liquid-over-solid (Figure 8.2.9) for the 300 in. waste with the peak mobilized extent reaching 68.4% of the solid.

The gas mobilization predictions, based on the strain limit and SEDL, are probably nonconservative for the reasons discussed above. The present predictions of 68% gas mobilization during the DBE might better represent 100% based on the SEDL.

The analyses of large deformation, elastic-plastic solid materials combined with hydrostatic fluid material modeling pushes the limits of ANSYS modeling capability. Considering the experience gained in exercising the ANSYS models, better answers could probably be obtained for the solid-over-liquid waste configuration by using a nonlinear analysis structural program that was developed specifically for this purpose. A more complete review of this modeling approach can be found in Section 9.

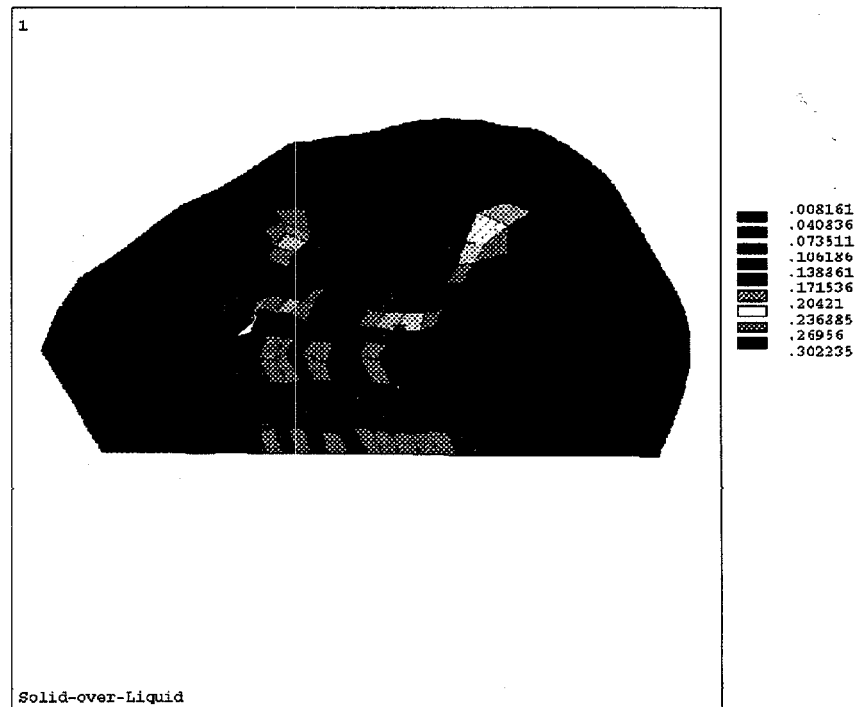


Figure 8.3.3. Peak Strain Energy Density (solid over liquid)

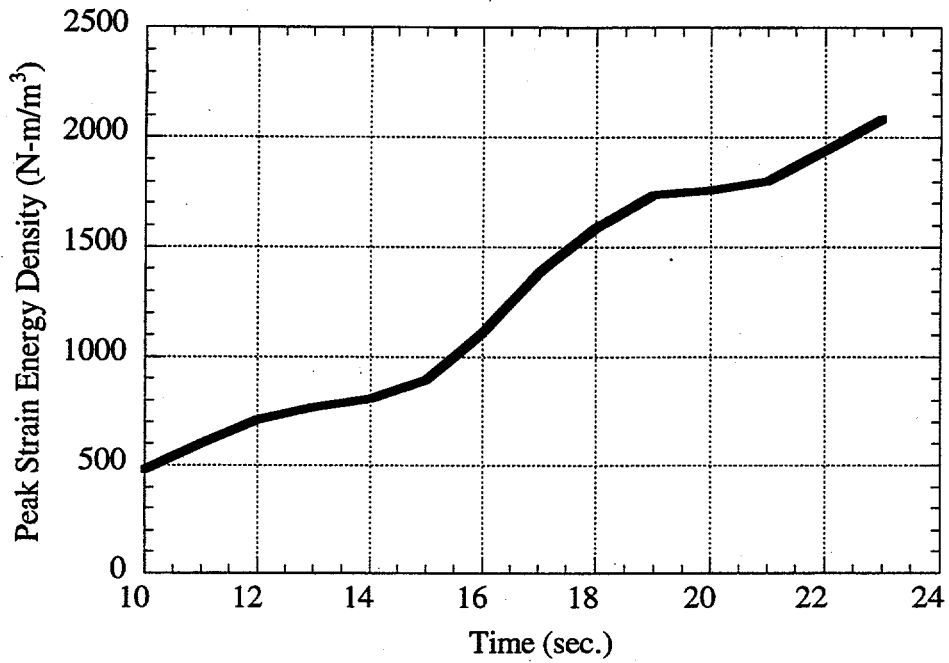


Figure 8.3.4. Time History of Waste Peak Strain Energy Density (solid over liquid)

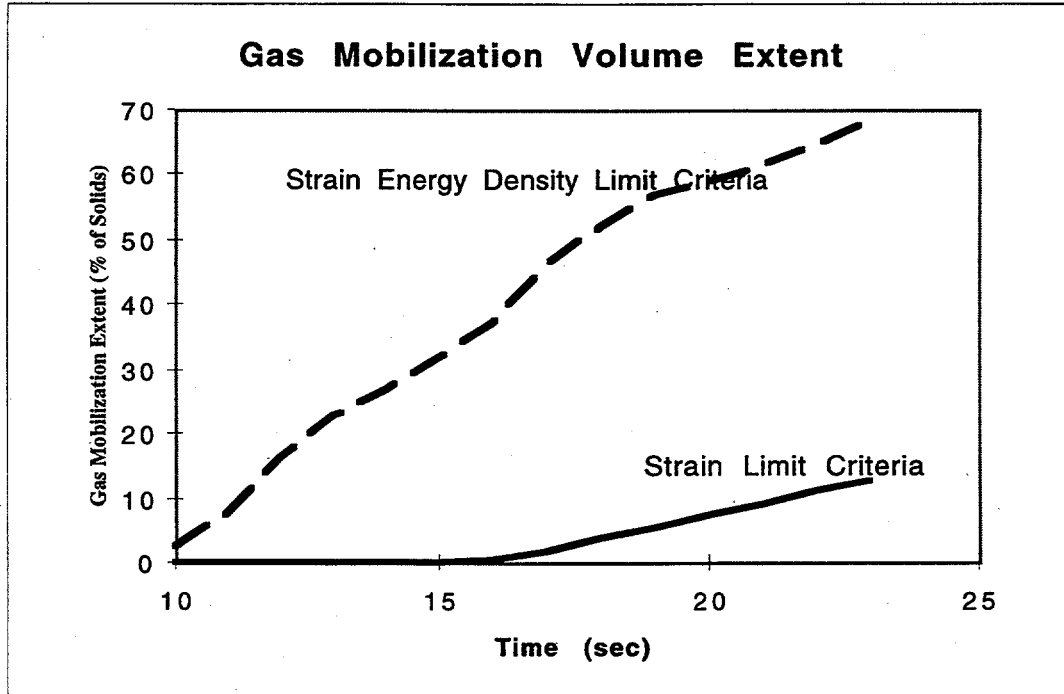


Figure 8.3.5. Time History of Volume Exceeding Strain Limit Criterion (liquid over solid)

The hydrostatic pressure pulses in the homogeneous and liquid-over-solid waste configurations also occur in the solid-over-liquid configuration. Figure 8.3.6 shows the strain energy density associated with the plastic shear strain and the elastic hydrostatic pressure waves for one location. The frequency of the waves is roughly 2 Hz, as in the other waste configurations.

These results confirm that using a highly incompressible elastic model for the liquid (pseudo-liquid in this case) embeds the hydrostatic pressure variations that are predicted by the ANSYS fluid element. The major variation with using the elastic solid element for the liquid is that shear occurs in the waste and reduces the harmonic oscillator amplification coupling to the waste solid modeled. One observation that can be drawn from the results is that, even with a liquid material bulk-to-shear modulus ratio of 10 orders of magnitude, enough shear occurs to dampen the solid waste excitation compared with a "pure fluid" liquid modeling.

8.4 Solid-over-Liquid-over-Solid Waste

The analyses of solid-over-liquid-over-solid configurations simulated the waste in Tank 241-AN-103 and used the ANSYS isoparametric element. This tank has a floating solids layer (crust) about one meter thick. The material model for the solid was identical to that used on the homogeneous waste with the same elastic-plastic yielding assumptions. For the liquid, an incompressible elastic material was used that was also used in the liquid-over-solid models. The solid-over-liquid waste model assumes that the waste in the tank is made up of an elastic-plastic solid medium covering a semi-incompressible elastic material. The solid portion of the waste alone is assumed to have a 12% gas volume fraction. The solid has a shear strength of 200 Pa based on ball rheometer data (Meyer et al. 1997), the lowest of any of the tanks modeled.

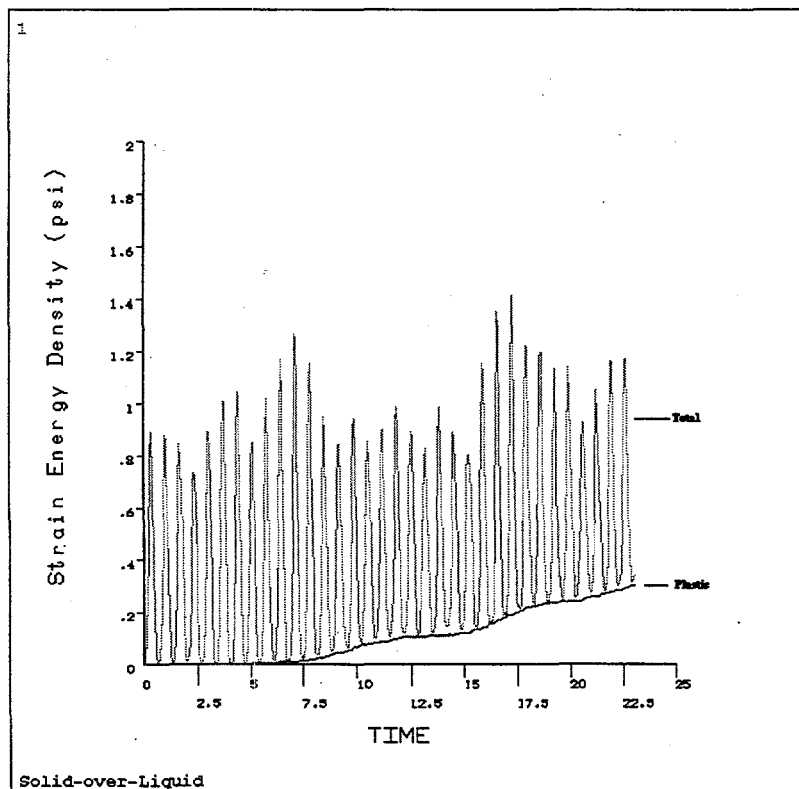


Figure 8.3.6. Time History of Peak Total and Plastic Strain Energy Density

In addition, the floating solids layer was assumed to behave like a solid of relatively low modulus. A shear modulus of 1,000 Pa and a density of 1,200 kg/m³ were assigned. For this analysis, the floating solid is assumed to remain an intact continuum material that does not break up but becomes plastic when effective strains exceed a 5% elastic limit. Basically, the floating layer simply adds hydrostatic pressure to the submerged solid waste with a very small stiffening effect. The material properties that are assigned for the solid and floating layers are shown in Table 8.4.1.

The predicted response of the solid exhibits the rapid transitions to plastic behavior observed in the liquid-over-solid configuration. The analysis became nonconvergent 6 or 7 seconds into the DBE with the use of ANSYS fluid element for the liquid. Converting the liquid material model to a very weak solid, as was done in the solid-over-liquid waste model, did not aid convergence. Since the waste has basically exceeded both of the gas mobilization criteria by 6 seconds into the DBE, the seismic simulation was terminated at this point. The liquid again acts as an elastic coupler generating hydrostatic pressures to the surface of the solid waste above. The floating solid does not stiffen the waste to any significant extent. The predicted peak strains in the solid layer are larger than those in the liquid-over-solid waste configuration. Figure 8.4.1 presents the time history of peak strains for this waste configuration. Only the strains in the lower solid layer are shown.

The predicted strain energy density is also much larger than in the other waste configurations. This is an indication that the use of a true fluid hydrostatic element tends to produce much more violence in overall waste motion than using a pseudo fluid, as was done with the solid-over-liquid waste model. The results suggest that solid-over-liquid waste model is nonconservative.

The peak strain energy density is 10⁵ N-m/m³. Figure 8.4.2 shows the predicted time history of peak strain energy density through part of the DBE. In addition to the liquid, the floating solids layer adds to the hydrostatic head. From the results of the liquid-over-solid waste modeling, the effect of increasing hydrostatic head is to increase the liquid oscillator coupling. Therefore, the amplification of solid waste response during the DBE is more severe than the equivalent liquid-over-solid response for similar waste depths.

Table 8.4.1. Material Properties of Solid-over-Liquid-over-Solid Waste

Elastic Yield Strain Limit		5%
Shear Modulus (Pa)	- solid	200
	- floating	1,000
Mean Depth Bulk Modulus	- solid	3,622,000
	- floating	
Young's Modulus (Pa)	- solid	18,013
	- floating	
Tensile Strength (Pa)	- solid	900
	- floating	
Poisson's Ratio	- solid	0.4974
	- floating	0.400

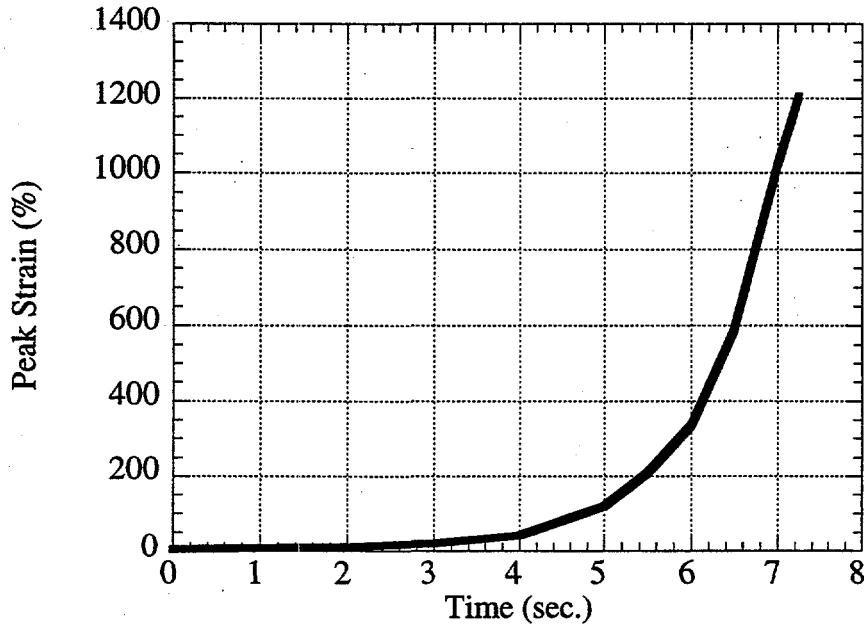


Figure 8.4.1. Time History of Peak Shear Strain (solid over liquid over solid)

The predicted gas mobilization based on the volume of waste exceeding the strain limit is virtually 100% at the end of 7 seconds based on either the strain limit criterion or the strain energy limit criterion. Figure 8.4.3 presents the time history of solid volume fraction mobilized. The waste becomes completely mobilized near the beginning of the DBE event, and its motion beyond 7 seconds is no longer tractable by classic structural analysis techniques because of the enormous plastic strains developing.

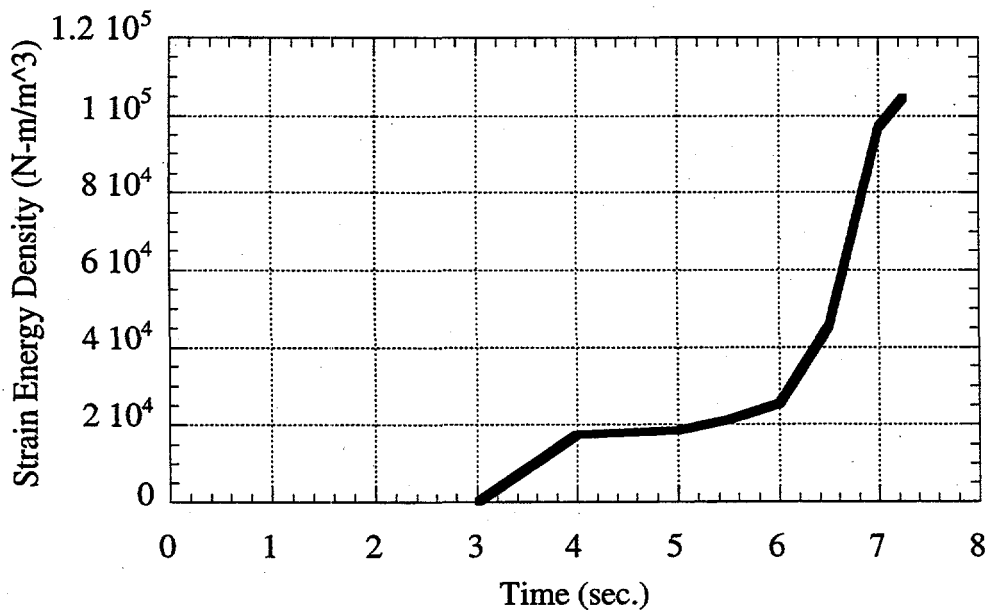


Figure 8.4.2. Time History of Peak Strain Energy Density (solid over liquid over solid)

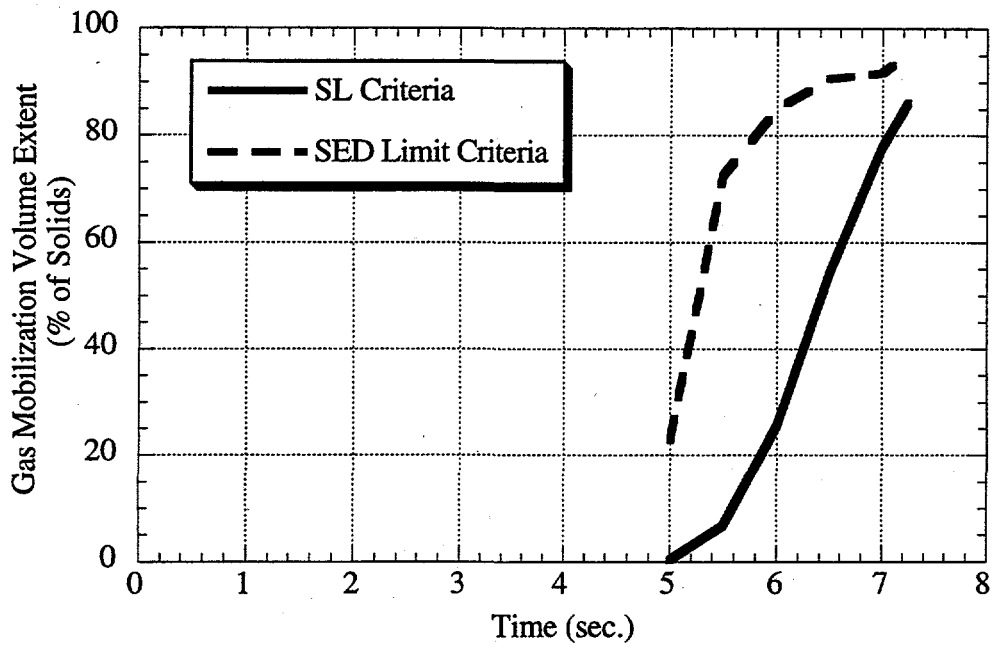


Figure 8.4.3. Time History of Volume Exceeding Strain Limit and Strain Energy Limit (solid-over-liquid-over-solid)

9.0 Conclusions and Recommendations

The response of four different waste configurations to a postulated 1,000-year DBE was studied by transient structural analysis using actual displacement boundary conditions at the tank wall. The waste configurations represented typical DSTs, a DST with a thick floating solids layer (241-AN-103), a typical SST with homogeneous waste, and an SST with a floating solid-over-liquid waste (241-A-101). While the extreme plastic strains and large hydrostatic pressure waves indicate that the analysis pushed the limit of structural analysis, the results give some very important insights into the potential gas releases from tanks subject to severe seismic events. They also point to additional studies and modeling improvements necessary to better quantify the potential for seismically induced gas release.

9.1 Summary of Gas Release Estimates

To first order, gas release volume is related to the volume of waste mobilized during the DBE. If bubbles could be assumed to rise through the mobilized waste as they would in a liquid, and if a mobilized path could be assumed to exist all the way to the waste surface, the fraction of retained gas released would be essentially equal to the fraction of the total waste volume mobilized. In fact, we would expect the actual configuration of the mobilized region and the non-Newtonian rheology of the waste to reduce the extent and rate of gas release into the dome space. A best estimate might be that half of the retained gas would be released from the mobilized solids layer. However, the first-order prediction that the fraction of the retained gas released equals the fraction of solids mobilized would be conservative.

The fraction of the solids volume mobilized based on the strain energy density criterion is summarized in Table 9.1 for each of the four waste configurations studied. The fraction of solids volume exceeding the SEDL is a measure of the potential gas release. However, these values must be used with caution. We can only conclude that a small value implies a small gas release and that a large value implies a large gas release—not that a specific fraction of the gas will be released.

Table 9.1. Summary of Fraction of Solids Volume Mobilized Based on SEDL

Waste Configuration	Solid Shear Strength (Pa)	Solids Depth (in.)	Liquid Depth (in.)	Total Waste Depth (in.)	Solids Volume > SEDL (%)
Homogeneous (SST)	300	150	0	150	5
	300	300	0	300	13
	6,000	150	0	150	0
	6,000	300	0	300	0
Liquid-over-Solid (DST)	300	150	150	300	98
	300	200	200	400	80
	6,000	150	150	300	0
	6,000	200	200	400	0
Solid-over-Liquid (A-101)	300	165	198	363	68
Solid-Liquid-Solid (AN-103)	200	36:149 ^(a)	163	348	~100 ^(b)

(a) Floating solid and lower solid layer depths, respectively.
 (b) At ~7 seconds into the 23-second transient. Simulation became unstable due to high plastic strain afterward.

For the homogeneous waste configuration, virtually none of the 6,000 Pa waste exceeds the strain energy density limit criterion. Only the weakest waste (300 Pa shear strength) broaches this limit but in less than 15% of the volume. We conclude that a "typical" SST without a supernatant liquid layer would be relatively immune to seismically induced gas releases, at least up to the 1,000-year DBE level.

The presence of any significant liquid layer, whether above or below the solids, tends to amplify the waste response, leading to much greater waste mobilization and gas release. However, the 6,000 Pa shear strength waste is apparently strong enough to resist mobilization even with a liquid layer present. The liquid-over-solid waste configuration showed almost complete mobilization for 300 Pa shear strength solids for both waste heights.

The addition of a floating solids layer on top of the liquid apparently makes the amplifying effect even stronger. The solid-over-liquid-over-solid case, which represents a DST with a thick floating solids layer (specifically 241-AN-103) reached complete mobilization after only 7 seconds. These results indicate that the predictions of earlier work (Stewart et al. 1996, based on spectrum shock method) indicating large gas release fractions from DSTs for even a 100-year earthquake are sound.

The solid-over-liquid waste configuration, representing Tank A-101, develops somewhat less, though still significant mobilization. However, these results may be non-conservative because of the "quasi-solid" model that had to be used to model the liquid for computational stability. It is probably prudent to conclude that a tank like A-101 would respond to an earthquake like a DST with a large gas release.

The results in Table 9.1 represent the response of the waste to a 1,000-year DBE. We can only make a very qualitative extrapolation to 100-year or 10,000-year DBEs. It is likely that there would be no gas release at all from homogeneous waste in a 100-year event. A 10,000-year DBE would almost certainly result in increased gas release from the homogeneous waste, but how much more cannot be estimated. For the other waste configurations with a liquid layer, it is unlikely that a 10,000-year event would increase the gas release much beyond the result of the 1,000-year DBE since mobilization is already near 100%. We cannot estimate how much less gas would be released in a 100-year event, or if there would be a decrease at all.

9.2 Conclusions

There are several general conclusions that apply to all waste configurations:

- The solid waste layers exceed the assumed elastic limit of 5% and become plastic everywhere during the DBE.
- Possibly the most important result is that a large portion of the seismic energy imparted to the waste is dissipated in large surface displacements or waves.
- A companion trend is that very large but localized plastic strains occur at what appear to be resonant points in the tank waste.
- A liquid layer acts as an elastic amplifier that drives the solid waste layers to much greater mobilization and potential for gas release for any given overall waste depth and strength.
- On the other hand, a homogeneous solid waste without a liquid layer resists mobilization since the entire waste volume develops shear stresses that absorb energy and damp waste motion. Seismic gas release from most SSTs may be minimal.

The weaker solid waste exhibits greater potential for mobilization. Solid layers with 300 Pa shear strength showed some mobilization for all waste heights over 150 inches. No solid material with a 6,000 Pa shear strength experienced any mobilization potential for waste heights up to 400 inches, although it developed some plastic strain throughout. This was true for both the strain limit and the strain energy limit criteria.

The strain energy density limit (SEDL) mobilization criterion was more conservative (i.e., predicted a greater waste volume mobilized over the DBE) than the strain limit (SL). Both of these criteria were derived assuming a 100% strain limit. The actual bound probably lies between 50% and 200% shear strain depending on waste. The SEDL is conservative because the strain energy limit could be exceeded before the equivalent strain limit. In the material model for plastic strain, the assumption was made that the "unloading" in the stress-strain relationship followed the elastic modulus (a classic engineering assumption). For this reason, tension and compression could overlap so that the strain energy would build without continuous increase in absolute strain.

The response of waste generally follows the classic relationship for beam stiffness. For any particular tank waste configuration, the effective stiffness is roughly proportional to the square root of the shear modulus divided by the square of the tank depth. Increased tank depth increases the mobilization and gas release potential. Decreasing the shear modulus does the same.

The waste mobilization and gas release criteria are based on shear strain. During the evaluation of waste response to postulated DBE, all models showed harmonic hydrostatic pressure waves, which produced stresses substantially greater than the shear stress limits associated with shear strain limit criteria. The lack of definitive data for gas mobilization based on deviatoric (shear) and dilatational (hydrostatic) stresses and strains makes it almost impossible to determine what significance the pressure waves has on potential gas release. For this reason, waste mobilization due to hydrostatic pressures was not considered in this study.

Finally, it is important to recognize that there is no direct connection between the motion (accelerations, velocities, or displacements) described by the response spectra input and the energy imparted during a seismic event. Appendix A outlines the power definition that can be determined from a response spectrum. When the response spectrum is converted to a power spectral density motion, only the power per unit of excited mass is prescribed. Therefore, the energy imparted to a material body (as waste) is dependent upon how the mass resonates or couples with the excitation. In the case of a rigid mass, the energy per unit time would depend simply on its total mass. Otherwise, the energy must depend on the integrated differential mass response.

9.3 Recommendations

A fundamental need is for greater understanding of yielding behavior of actual waste. The mechanism of material failure was assumed to be related to shear stress-strain. But large hydrostatic pressure waves are predicted to occur in which the associated dilatational stresses are much larger than the shear stresses produced. Since typical engineering materials do not typically fail because of hydrostatic pressure, there are no readily available prescriptions to a failure model for waste containing bubbles. Differentiation between shear and hydrostatic stresses on yielding needs to be quantified. We infer that many waste materials exhibit a continuum solid mechanics character to hydrostatic stresses. There is actually insufficient mechanical property data to ascertain the degree to which this is true. A general solid mechanics material model needs to be developed for waste material based on such properties as solids content, density, and viscosity.

The present material modeling uses von Mises stresses derived from a maximum energy density limit, to determine material yielding (elastic limit). The material yielding models in ANSYS

typically employ some form of principal stress, shear stress, or distortion energy formulation in predicting failure. It is feasible to develop alternate failure modeling by using "user defined" macro routines. Some consideration might be given to developing a pure strain limit criterion or hydrodynamic stress limit criterion for failure. Recent studies of hydrostatic sonification of solid/bubble media suggest that cyclic hydrostatic waves with pressure amplitudes between one the ten times the material shear strength can mobilize trapped gas.^(a) Analyses of DBE seismic events using one of these material models would provide a contrast to von Mises based yielding criteria.

Large deformation elastic-plastic analyses with combined hydrostatic fluid material modeling has likely pushed beyond the limits of ANSYS modeling capability. Future modeling of waste motion where a large portion is a fluid that exhibits significant hydrostatic pressure variations probably should consider using lagrangian mechanics codes like MARC (MARC 1997) or ABACUS (Hibbitt et al 1997).

Alternate waste response analyses that consider fluid mechanics (stresses induced by the strain rate) could be employed for predicting waste mobilization. PNNL has employed nonlinear, non-Newtonian fluid flow analyses of waste in tanks to model buoyant displacements and the effects of pump jets. However, direct application of time-dependent seismic displacements or accelerations is not convenient for fluid dynamics models. Some computational fluid dynamics (CFD) software with moving boundary capability might allow for displacement boundary conditions, but it is neither trivial nor a sure thing that a real or converged prediction could be obtained.

The major objection to CFD methodology in predicting yielding of non-Newtonian fluids is that they lack zero strain rate yielding modeling capability. CFD programs typically employ a non-Newtonian model of the Bingham plastic material form. True Bingham fluid models require a finite stress at zero strain rate to yield the material. Because the basis of CFD is strain rate (velocity) induced stress, ad hoc techniques are used in practice to predict pseudo-stress yielding via velocity and avoid this ambiguity.

A more appropriate method might be to combine solid and fluid mechanics techniques to model waste. One possible way to do this would be to treat local discretized space as strain-induced stresses up to some mechanical condition (such as shear strain). A procedure would then convert a discrete element into non-Newtonian fluid whereby the laws governing its motion are fluid based. Application of appropriate boundary conditions would still require an appropriate modeling technique, but moving boundaries or conversion to force (or pressure) might be an adequate method.

(a) Lessor DL. *Applicability of a Single Sonic Probe to Retrieval Enhancement in Hanford Waste Tank 241-SY-102*. Letter Report, Pacific Northwest National Laboratory, Richland, Washington.

10.0 References

Avallone EA and T Baumeister, eds. 1987. *Marks Standard Handbook for Mechanical Engineers*. McGraw-Hill, New York.

Gauglitz PA, SD Rassat, MR Powell, RR Shah, and LA Mahoney. 1995. *Gas Bubble Retention and Its Effects on Waste Properties: Retention Mechanisms, Viscosity, and Tensile and Shear Strengths*. PNL-10740, Pacific Northwest National Laboratory, Richland, Washington.

Hibbitt, Karlsson and Sorensen, Inc. 1997. *The ABACUS Finite Element Program*. Hibbitt, Karlsson and Sorensen, Pawtucket, Rhode Island.

Hughes WF and EW Gaylord. 1964. *Basic Equations of Engineering Science*. Schaum's Outline Series, McGraw Hill, New York.

Kohnke PC, ed. 1994. *Engineering Analysis System, Theoretical Manual*. Swanson Analysis System, Inc, Houston, Pennsylvania.

Malvern LE. 1969. *Introduction to the Mechanics of a Continuous Medium*. Prentice-Hall Inc., Englewood Cliffs, New Jersey.

MARC Analysis Research Corporation. 1997. *The MARC Finite Element Program, Revision K6.2*. MARC Analysis Research Corporation, Palo Alto, California.

Meyer PA, ME Brewster, SA Bryan, G Chen, LR Pederson, CW Stewart, G Terrones. 1997. *Gas Retention and Release Behavior in Hanford Double-Shell Tanks*. PNNL-11536, Pacific Northwest National Laboratory, Richland, Washington.

Newmark NM and WJ Hall. 1978. *Development of Criteria for Seismic Review of Selected Nuclear Power Plants*. NUREG/CR-0098, U.S. Nuclear Regulatory Commission, Washington, D.C.

Shekarriz A, DR Rector, LA Mahoney, MA Chieda, JM Bates, RE Bauer, NS Cannon, BE Hey, CG Linschooten, FJ Reitz, and ER Siciliano. 1997. *Composition and Quantities of Retained Gas Measured in Hanford Waste Tanks 241-AW-101, A-101, AN-105, AN-104, and AN-103*. PNNL-11450, Pacific Northwest National Laboratory, Richland, Washington.

Stewart CW, LA Schienbein, JD Hudson, EJ Eschbach, and DL Lessor. 1994. *Assessment of Alternative Mitigation Concepts for Hanford Flammable Gas Tanks*. PNL-10105, Pacific Northwest Laboratory, Richland, Washington.

Stewart CW, ME Brewster, PA Gauglitz, LA Mahoney, PA Meyer, KP Recknagle, and HC Reid. 1996. *Gas Retention and Release Behavior in Hanford Single-Shell Waste Tanks*. PNNL-11391, Pacific Northwest National Laboratory, Richland, Washington.

U.S. Department of Energy. April 1994. *Natural Phenomena Hazards Design and Evaluation Criteria for Department of Energy Facilities*. DOE Standard STD-1020-94.

Weiner, EO and AC Rohay. 1992. *Design Basis Earthquake Time Histories for 1992 SDC-4.1, Revision 12*. WHC-SD-GN-30018, Westinghouse Hanford Company, Richland, Washington.

Whitney PD, PA Meyer, NE Wilkins, F Gao, and AG Wood. 1996. *Flammable Gas Data Evaluation Progress Report*. PNNL-11373, Pacific Northwest National Laboratory, Richland, Washington.

Wilkins NE, RE Bauer and DM Ogden. 1997. *Results of Vapor space Monitoring of Flammable Gas Watch List Tanks*. HNF-SD-WM-TI-797 Rev. 1, Lockheed MartinHanford Company, Richland, Washington.

Zienkiewicz OC, C Humpheson, and RW Lewis. 1975. "Associated and Non-Associated Visco-Plasticity and Plasticity in Soil Mechanics." *Geotechnique*, Vol. 25.

Appendix

Energy Associated with the Spectrum DBE Event

Appendix

Energy Associated with the Spectrum DBE Event

The frequency spectra outlined in *Design Basis Earthquake Time Histories for 1992 SDC-4.12* (Weiner and Rohay 1992) can be converted into power spectra conditions. Power spectral density (PSD) represents power (energy/time) given at a particular frequency for random vibration acceleration. The power from a random harmonic vibration can be derived based on converted PSD curves for the DBE acceleration (or velocity) relationships for harmonic motion. Assuming that the motion obeys harmonic motion laws, velocity can be defined as

$$a = v f_{\omega}$$

where f_{ω} is the frequency of the harmonic. Newton's law of momentum can be written as

$$\frac{F}{m} = a$$

and energy is force through a distance, so energy-per-unit-mass is

$$\frac{E}{m} = \frac{F \cdot d}{m}$$

and therefore power (as energy/time) is

$$\frac{P}{m} = \frac{F}{m} \frac{d}{t} = \frac{FV}{m} = a \frac{a}{f_{\omega}}$$

This is specific power and has the units of power/mass (N-m/kg-s or ft-lb/lbm-sec). The definition of PSD is the change in the mean square value of the excitation with respect to frequency, or

$$W = \frac{d \bar{g}^2(f)}{d f}$$

where $g(f)$ is the frequency dependent acceleration spectra. PSD is typically written as

$$W(f) = g^2(f)/f$$

where g is the acceleration and f is the frequency associated with it. Figure A.1 presents the converted PSD for the postulated DBE 2% damped spectrum. This is a standard interpretation of power defined by a spectral density curve; detailed derivation is developed by Harris (1988).

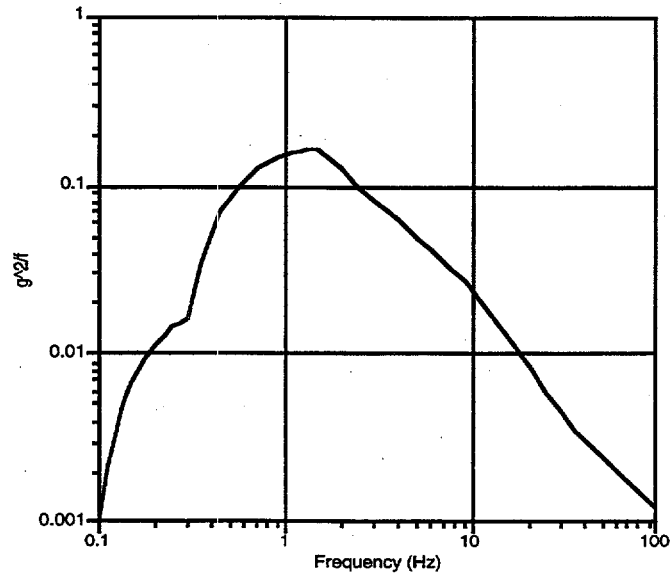


Figure A.1. Power Spectral Density Conversion of the 2% Damped Hanford DBE Spectrum

The total energy from the DBE, assuming a 23-second transient and invariant spectrum over that time, can be estimated from the average power by

$$\frac{E}{m} = \overline{W} * t.$$

This energy definition is also employed by Weiner and Rohay (1992) in Section 4.2 for Hanford DBE events. The power is frequency averaged using the root-mean-square excitation so that

$$\overline{W} = \frac{\int W_{RMS}(f_d) df}{\int df}$$

Performing this integration and converting to total energy/mass

$$E/m = 23 \text{ seconds} (0.32744 \text{ ft-lb/lb-sec}) = 7.53 \text{ ft-lb/lb,m}$$

Therefore, an acceleration response specifies energy per unit time and per unit mass of material in motion. A unique energy per unit time (power) is not independent of the mass undergoing excitation.

References

Harris CM. 1988. *Shock and Vibration Handbook* (third edition). McGraw-Hill, New York.

Weiner, EO and AC Rohay. 1992. *Design Basis Earthquake Time Histories for 1992 SDC-4.1, Revision 12*. WHC-SD-GN-30018, Westinghouse Hanford Company, Richland, Washington

Distribution

<u>No. of Copies</u>	<u>No. of Copies</u>
Offsite	
2	2 Los Alamos National Laboratory P.O. Box 1663 Los Alamos, NM 87545 Attn: D. Bennett K575 C. Unal K575 D. Pepson U.S. Department of Energy Trevion II Building, EM-35 Washington, DC 20585-0002 Scott E. Slezak 806 Hermosa NE Albuquerque, NM 87110 D. A. Powers Sandia National Laboratories MS-0744 Albuquerque, NM 87185-0744 A. B. Stone Washington Dept. of Ecology 1315 W. 4th, B5-18 Kennewick, WA 99336 J. Tseng U.S. Department of Energy Trevion II Building, EM-35 Washington, DC 20585-0002
2	DOE Office of Scientific and Technical Information D. Campbell 102 Windham Road Oak Ridge, TN 37830 C. W. Forsberg Oak Ridge National Laboratory P.O. Box 2008, MS-6495 Oak Ridge, TN 37831-6495
2	Westinghouse Savannah River Co. Savannah River Site Aiken, SC 29802 Attn: S. J. Eberlein 271-121H B. Hester 703H
	B. C. Hudson P.O. Box 271 Lindsborg, KS 67456 M. S. Kazimi MIT Department of Nuclear Engineering 77 Massachusetts Avenue Cambridge, MA 02139
	J. L. Kovach P.O. Box 29151 70000 Huntley Road Columbus, OH 43229
	T. S. Kress 102-B Newridge Road Oak Ridge, TN 37830
	T. E. Larson 2711 Walnut St. Los Alamos, NM 87545
	Onsite 2 <u>DOE Richland Operations Office</u> C. A. Groendyke S7-54 G. W. Rosenwald S7-54 24 <u>Project Hanford Management Team</u> S. A. Barker R2-11 W. B. Barton R2-12 R. E. Bauer S7-14 D. R. Bratzel S7-14 R. J. Cash S7-14

No. of
Copies

No. of
Copies

PHMC (contd)

31 Pacific Northwest National Laboratory

N. W. Kirch	R2-11
J. W. Lentsch	S2-48
J. M. Grigsby	S7-14
G. D. Johnson (10)	S7-14
R. M. Marusich	A3-34
D. A. Reynolds	R2-11
E. R. Siciliano	HO-31
L. M. Stock	S7-14
R. J. Van Vleet	A3-34
J. R. White	S7-15

Z. I. Antoniak	K7-15
J. M. Bates	K7-15
S. Q. Bennett	K7-90
J. W. Brothers	K9-20
J. E. Deibler	K5-26
P. A. Gauglitz	P7-41
K. I. Johnson	K5-26
L. A. Mahoney	K7-15
P. A. Meyer	K7-15
L. M. Peurrung	P7-41
A. C. Rohay	K6-81
H. C. Reid (10)	K7-15
C. W. Stewart (5)	K7-15
Information Release (5)	K1-06